King Saud University

Arabian Journal of Chemistry

www.ksu.edu.sa
www.sciencedirect.com

ORIGINAL ARTICLE

Exploring the effective components and potential mechanisms of Zukamu granules against acute upper respiratory tract infections by UHPLC-Q-Exactive Orbitrap-MS and network pharmacology analysis

Kailin Li [a,b,1], **Qian Yao** [a,1], **Min Zhang** [b], **Qing Li** [b], **Lilan Guo** [b], **Jing Li** [b], **Jianbo Yang** [c,d,*], **Wei Cai** [a,b,*]

[a] *Weifang Medical University, Weifang 261053, China*
[b] *Hunan Province Key Laboratory for Antibody-based Drug and Intelligent Delivery System, School of Pharmaceutical Sciences, Hunan University of Medicine, Huaihua 418000, China*
[c] *National Institutes for Food and Drug Control, Beijing 100050, China*
[d] *Xinjiang Uygur Autonomous Region Institute for Drug Control, Urumqi 830054, China*

Abstract Acute upper respiratory tract infections (AURTIs) are common diseases of respiratory system, which are caused by adenoviruses and generate the mix of severe clinical presentation. Zukamu granules (ZKMG), a traditional Chinese medicine (TCM) prescription within Health Commission of Xinjiang Uygur Autonomous Region possesses anti-influenza virus, antibacterial and anti-inflammatory effects that exerts therapeutic effects in treatment of AURTIs. However, the main effective chemical components and their corresponding action mechanisms have not been clarified. Therefore, ultra-performance liquid chromatography coupled with quadrupole Exactive orbitrap tandem mass spectrometry (UHPLC-Q-Exactive Orbitrap MS) and network pharmacology were used to detect and identify potentially effective components in ZKMG as well as uncover

---

* Corresponding authors at: Hunan Province Key Laboratory for Antibody-based Drug and Intelligent Delivery System, School of Pharmaceutical Sciences, Hunan University of Medicine, Huaihua 418000, China (W. Cai), National Institutes for Food and Drug Control, Beijing 100050, China; Xinjiang Uygur Autonomous Region Institute for Drug Control, Urumqi 830054, China (J.B. Yang).
 E-mail addresses: yangjianbo@nifdc.org.cn (J. Yang), 20120941161@bucm.edu.cn (W. Cai).
 [1] These authors contributed equally to this work.

ELSEVIER | **Production and hosting by Elsevier**

their pharmacological mechanisms against AURTIs. As a result, a total of 265 components from all 12 composed herbal medicines were characterized based on self-built database and fragmentation patterns, of which 38 compounds were unambiguously confirmed using reference standards. Then, the compound-target-pathway network was constructed that implied potential therapeutic mechanisms of ZKMG on AURTI. Compounds noscapine, cryptopine, steviol-19-O-glucoside, N-methylnarcotine, allocryptopine, naringenin, boldine, methyl rosmarinate with related targets EGFR, PTGS2, IL2, MMP9, TNF, AKT1, PIK3CA, F3 were considered as the key components and targets. Besides, the results also indicated that PI3K-Akt, AGE-RAGE, PD-L1, HIF-1 signaling pathways contributed significantly to the therapeutic effects of ZKMG on AURTIs. Overall, ZKMG could have an effect on AURTIs based on multicomponent, multitarget, and multichannel mechanisms of action as well as this method provides guiding significance for the further development of TCM treatment.

1. Introduction

Acute upper respiratory tract infections (AURTIs) are one of the most common respiratory infectious diseases characterized by tonsillitis, pharyngitis, laryngitis, rhinitis, angina and the common cold, which are primarily caused by viruses rather than bacteria, fungi, and helminths (Huang et al., 2019; Xu et al., 2022). It was reported that the global incidence of AURTIs was 17.1 billion worldwide in 2017, which has brought about tremendous socioeconomic burden to public health (James et al., 2018). Although, the majority of AURTIs are slight and self-limited, they could result in undesirable clinical outcomes, as well as their complications might develop into serious diseases and threaten the security of the infected (Huang et al., 2019). The conventional treatment for AURTIs are preliminary medicines that relieve symptoms but do not treat disease infections, such as antipyretic analgesics and antihistamines (Pelzman and Tung, 2021). Antibiotics only for specific AURTIs and validated clinical indications are recommended, but most of antibiotics for common AURTIs are needless and ineffective (Wang et al., 2014; Harris et al., 2016; Zhang et al., 2021). Additionally, the inappropriate utilization of antibiotics could lead to the emergence of resistant bacteria and increase treatment difficulties in clinical practice (Alrafiaah et al., 2017). Therefore, it is necessary that new therapeutic drugs are explored for AURTIs treatment.

Traditional Chinese medicine (TCM) has the advantages of low toxicity and less adverse reactions, reversing multidrug resistance and reducing drug dosage, which has been widely considered to be effective method for various diseases because of its characteristics of multicomponents and multitargets (Chen et al., 2021; Kong et al., 2021). It is by using TCM that AURTIs have been cured for more than 1800 years in China and TCM plays a significant role in disease prevention (Zeng et al., 2022). Zukamu granules (ZKMG) as a famous classical formula was first recorded in the Uyghur medical book karibatin kader over 1500 years ago, which was known as the first choice for the treatment of colds in Uighur (Hou et al., 2019; Zeng et al., 2021). ZKMG is composed of *Kaempferia galanga* (KG), Pericarpium papaveris (*Papaver somniferum*) (PP), *Matricaria recutita* (MR), *Ziziphus jujuba* (ZJ), *Mentha canadensis* (MC), *Glycyrrhiza uralensis* (GU), *Althaea rosea* (AL), *Nymphaea tetragona* (NT), *Rheum palmatum* (RP), *Co rdia dicholoma* (CRD) (Zeng et al., 2021). Modern pharmacological studies have revealed that ZKMG exhibits preferable anti-inflammatory anti-oxidant stress, regulation of apoptosis, and analgesic activities, as well as it is widely used for treating AURTIs and lung diseases in clinical studies (Li et al., 2022). Alkaloids in PP, flavonoids in ZJ, saponins in GU and quinones in RP have been primarily regarded as the main components of ZKMG prescription herbs. Besides, these components have been found to possess pharmacological activities against AURTI (Fiore et al., 2008; Song et al., 2014; Liu et al., 2015; Parsaei et al., 2016). However, as a complex TCM prescription, the therapeutic effect of ZKMG is not a function of a single herb as well as active compounds and action mechanism in the treatment of AURTIs remain still unclear because of the multichemical components, multi-pharmacological effects, and multi-action targets of ZKMG, so it is quite necessary to explore the potential pharmacodynamic substances and mechanism, which are related to its therapeutic function.

Apparently, the diversity of the chemical constituents of TCM possibly results in complex interactions between active ingredients and multiple targets in diseases. It is a great challenge that how to comprehensively explore potential effective constituents and mechanisms of action (Huang et al., 2021). Ultra-high performance liquid chromatography coupled with quadrupole-Exactive orbitrap mass spectrometry (UHPLC-Q Exactive Orbitrap-MS) is powerful qualitative analysis technique, which has been developed for rapid characterization of unknown trace components in herbal medicines due to its high sensitivity, high resolution and high selectivity (Wang et al., 2021). Network pharmacology could systematically illustrate complex interactions among drugs, chemical constituents, targets, diseases and pathways, which has been considered to be a reliable approach to predict the pharmacological mechanism of drug treatments for diseases based on the development of systems biology and bioinformatics (Lu et al., 2021).

Therefore, it is a powerful method that UHPLC-MS combined with network pharmacology was used to explore the active ingredients and their potential mechanisms of TCM formula. In this study, a rapid and sensitive UHPLC-Q Exactive Orbitrap-MS method was established to investigate complex chemical compounds of ZKMG and their related mechanisms were explored by network pharmacology analysis. The study has certain guiding significance for clinical use and exploration mechanisms of action of ZKMG in treatment of AURTIs.

2. Materials and methods

2.1. Materials and reagents

Zukamu granules (ZKMG) were provided by Xinjiang Uygur Pharmaceutical Co., Ltd. (220252, Xinjiang, China). The detailed information of reference standards is listed in Supplementary Table S1. Chromatographic grade methanol and acetonitrile were purchased from Merck (New Jersey, USA). Ultrapure water was prepared with a Milli-Q system (Millipore, Milford, MA, USA). LC-MS grade formic acid was obtained from Fisher Scientific (New Jersey, USA). All other reagents were of analytical grade.

2.2. Sample preparation

Zukamu granules (1 g) were extracted in 50 mL 70% (v/v) aqueous methanol with ultrasonic treatment for 1 h at 30 °C and 40 kHz. The extracting solution was filtered and evaporated (50 °C) using the rotary vacuum evaporator to obtain the residue of ZKMG. Then, 100 mg ZKMG extracts were approximately weighted and dissolved in 1 mL methanol. After centrifugation at 12000 rpm for 20 min, an aliquot (2 μL) of supernatant was injected into the UHPLC-MS system for analysis.

Individual stock solutions of standards (1 mg/mL) were respectively accurately weighted and prepared by dissolving in methanol. Then, the solutions of 38 standards were mixed and serially diluted at a concentration of 10 μg/mL stored at −20 °C before UHPLC-MS analysis.

2.3. UHPLC-MS conditions

Each sample was performed on an Ultimate 3000 system (Thermo Fisher Scientific, California, USA) equipped with an Thermo Scientific Syncronis C18 (100 mm × 2.1 mm, 1.7 μm) at a temperature of 45 °C. The mobile phases consisted of 0.1% formic acid in water (A) and acetonitrile (B), delivering at a flow rate of 0.3 mL/min with the following solvent gradient: 0–2 min, 95–92% A; 2–5 min, 92–85% A; 5–10 min, 85–78% A; 10–12 min, 78–50% A; 12–20 min, 50–35% A; 20–25 min, 35–20% A; 25–26 min, 20–95% A; 26–30 min, 95% A.

The UHPLC system was coupled to a Q-Exactive Orbitrap MS (Thermo Fisher Scientific, Bremen, Germany), equipped with a heated electrospray ionization source (HESI) in the negative and positive modes for detection with the mass range of m/z 120–1200. For the spray voltage, the positive ion mode was 3.5 kV and the negative ion mode was 3.0 kV. The MS^1 spectra were acquired with full MS mode with a resolution of 35,000, and the MS^2 spectra resolution was 17,500 conducted in the data-dependent acquisition (DDA) mode. The sheath gas flow rate of 30 arbitrary units and auxiliary gas flow rate of 10 arbitrary units; and the temperatures of the capillary and auxiliary gas heaters were kept at 320 and 350 °C, respectively. The acquisition mode of the stepped normalized collision energy was set to 30, 40, and 60 %. The mass data were analyzed by Xcalibur 4.2 software (Thermo Fisher Scientific, California, USA).

2.4. The UHPLC-MS data analysis of ZKMG

The approaches for identifying chemical composition of ZKMG were divided into three steps. (1) The self-built database based on searching compounds in domestic and international databases or related natural products research literatures, such as GoogleScholar, PubMed and CNKI, was established for consisted herbs of ZKMG including compounds names, molecular formulars, fragment ions and classifications. Besides, the fragmentation pathways of reference standards obtained were investigated to be beneficial for the characterization. (2) The Xcalibur 4.2 software was applied to acquire extracted ion chromatograms (EICs) of possible compounds, theoretical mass, experimental mass, retention times, mass error and detailed MS/MS fragment ions in both negative and positive modes. (3) The data pre-obtained from

(1) was extracted in experimental row data in Xcalibur 4.2 software to identify chemical profiles by matching MS/MS fragments. Furthermore, the fragmentation patterns of reference standards were used to characterize unknown components, which possess similar skeleton structures or fragment ions based on the principle of structural similarity (Fig. 1).

2.5. Network pharmacology analysis

Firstly, all the identified compounds based on UHPLC-MS were transformed into canonical SMILES through the PubChem (https://pubchem.ncbi.nlm.nih.gov/), most recently updated in March 2019. However, a number of compounds were not found in the PubChem, then their structures were imported in SwissTargetPrediction (http://www.swisstarget-prediction.ch/, updated in 2019) to obtain SMILES, and the canonical SMILES information was uploaded into the SwissTargetPrediction database in "homo sapiens" species to predict all potential targets of compounds with probability ≥ 0.1 as the screening condition (Daina et al., 2019). Then the target genes obtained were verified by the Uni-Prot protein database (https://www.uniprot.org/, updated in 2022) and converted into corresponding standard gene names (UniProt. 2018). Secondly, the keywords about "AURTIs" as well as relevant diseases "acute pharyngitis", "acute tonsillitis", "acute rhinitis", "acute laryngitis" and "acute angina" were searched to obtain AURTIs related gene targets from Online Mendelian Inheritance in Man database (OMIM http://omim.org/, updated in 2018) and GeneCards database (https://www.genecards.org/, version 5.0), and screen genes with "relevance score" of disease ≥ 30, and the repeated targets were deleted (Amberger et al., 2015; Stelzer et al., 2016). Thirdly, the chemical compounds targets and the diseases targets were imported in bioinformatics website (http://bioinformatics.psb.ugent.be/webtools/venn/, updated in 2022) to draw a Venn diagram and obtain their common gene targets. Then, the chemical components of ZKMG and its therapeutic targets in AURTIs were introduced into Cytoscape (https://cytoscape.org/, version 3.9.1) to construct the compound-target network (Shannon et al., 2003). Afterwards, the overlapping targets between the compounds targets and the AURTIs related targets were inputted into STRING database (http://string-db.org/, version 11.0) with a high confidence score ≥ 0.9 to construct the protein–protein interaction (PPI) network. The Cytoscape software (version 3.9.1) was used to visualize and analysis interactions in this network according to the network node topological parameter "degree", it was used for evaluating the importance in the PPI network of a protein (Szklarczyk et al., 2018; Zhuang et al., 2020). Finally, the Database for Annotation, Visualization and Integrated Discovery (DAVID https://david.ncifcrf.gov/, version 6.8) was used for GO enrichment including molecular function (MF), biological process (BP), cellular components (CC), and KEGG pathway analysis (https://www.bioinformatics.com.cn/, updated in 2022), which provided systematic and comprehensive biological function annotation information. Meanwhile, top 20 enriched pathways of three GO terms (MF, BP, and CC) and KEGG were visualized in a bubble chart as well as three GO terms were drawn together with a bar chart and represented by a box line partition (p < 0.01) (Huang da et al., 2009; Li et al., 2022). Compound-target-
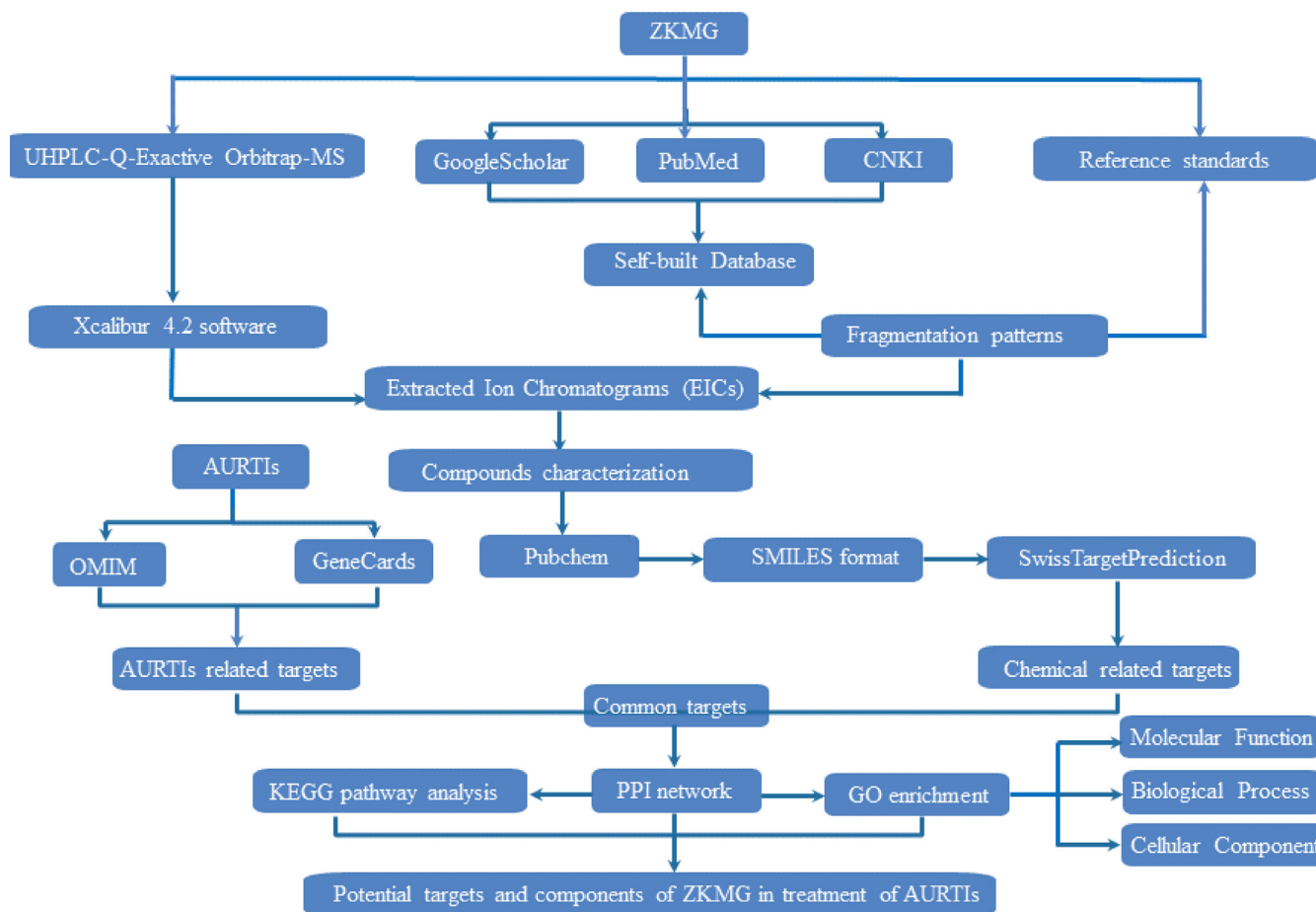
Fig. 1 The analytical strategy based on UHPLC-MS and network pharmacology for exploring potential pharmacodynamic substance and mechanisms of action of ZKMG on AURTIs.

pathway networks were constructed by using Cytoscape software (Fig. 1).

3. Results and discussion

3.1. Characterization of chemical components of ZKMG

The chemical ingredients of ZKMG were detected and identified by UHPLC-Q-Exactive Orbitrap MS in both positive and negative modes to obtain as much information as possible. Totally, 265 compounds were identified from ZKMG based on accurate precursor and product ions and comparing their fragmentation patterns with standards or reported in the literatures, including 46 alkaloids, 92 flavonoids, 28 triterpenoid saponins, 27 phenolic acids, 24 phenylpropanoids, 21 quinones, 13 tannins, 4 amino acids, 4 nucleosides, 2 naphthols, 2 phenols, 2 terpenoids in Table 1 and Supplementary Table S2. The extracted ion chromatograms (EICs) of these compounds in both positive mode and negative ion modes were showed in Fig. 2. And 38 compounds in ZKMG were unambiguously identified by comparison with reference standards.

3.1.1. Identification of alkaloids

In this study, a total of 46 alkaloids mainly derived from PP were identified, which could be further divided into different alkaloids, including 2 tetrahydroprotoberberines, 5 aporphines, 20 benzyltetrahydroisoquinolines, 5 phthalideisoquinolines, 6 protopines, 5 morphinans, 3 benzylisoquinolines. The proposed fragmentation pathways of each-type representative alkaloids (peaks **88**, **72**, **56**, **153**, **144**, **16**, **146**) were observed in Supplementary Figure S3.

3.1.1.1. Identification of tetrahydroprotoberberine alkaloids. Tetrahydroprotoberberine is a four-ring structure, which derived from two isoquinoline rings connected by sharing one nitrogen atom, and its C2, C3, C9, C10 contain oxygen groups (Yang et al., 2016). The peaks **88** and **112** were deemed to be tetrahydroprotoberberine alkaloids because of their MS/MS spectral patterns, which produced characteristic ions by Retro Diels-Alder (RDA) cleavage. They were tentatively identified as scoulerine and tetrahydrocolumbamine based on MS/MS fragmentation pattern of tetrahydroprotoberberine alkaloids. The fragmentation ions of scoulerine and tetrahydrocolumbamine were observed at *m/z* 178.086

Table 1 Identification of chemical components in ZKMG by UHPLC-Q-Exactive Orbitrap MS.

peak	t_R	Theoretical Mass m/z	Experimental Mass m/z	Error (ppm)	Formula	Identification	peak	t_R	Theoretical Mass m/z	Experimental Mass m/z	Error (ppm)	Formula	Identification
1*	0.84	136.0618	136.0617	−0.68	$C_5H_5N_5$	adenine	134	10.37	463.0882	463.0888	1.31	$C_{21}H_{20}O_{12}$	quercetin-7-O-glucoside
2*	0.84	191.0561	191.0553	−4.19	$C_7H_{12}O_6$	quinic acid	135	10.41	477.0675	477.0680	1.04	$C_{21}H_{18}O_{13}$	quercetin-3-O-glucuronide
3	0.90	191.0197	191.0190	−3.80	$C_6H_8O_7$	citric acid isomer	136*	10.47	463.0882	463.0888	1.32	$C_{21}H_{20}O_{12}$	isoquercitrin
4*	0.92	133.0142	133.0132	−8.24	$C_4H_6O_5$	malic acid	137	10.52	447.0933	447.0931	−0.45	$C_{21}H_{20}O_{11}$	luteolin-5-O-glucoside
5	1.05	191.0197	191.0190	−3.80	$C_6H_8O_7$	isocitric acid	138	10.55	445.0776	445.0781	1.02	$C_{21}H_{18}O_{11}$	rhein-8-O-β-D-glucoside
6*	1.18	191.0197	191.0190	−3.75	$C_6H_8O_7$	citric acid	139*	10.66	447.0933	447.0937	0.91	$C_{21}H_{20}O_{11}$	cynaroside
7	1.28	331.0671	331.0674	1.03	$C_{13}H_{16}O_{10}$	1-O-galloylglucose	140	10.66	461.0725	461.0730	0.91	$C_{21}H_{18}O_{12}$	kaempferol-3-O-β-D-glucuronide
8	1.31	268.1040	268.1038	−1.01	$C_{10}H_{13}N_5O_4$	adenosine	141*	10.69	623.1981	623.1988	1.04	$C_{29}H_{36}O_{15}$	acteoside
9	1.32	132.1019	132.1019	−0.19	$C_6H_{13}NO_2$	isoleucine	142	10.87	615.0992	615.1002	1.63	$C_{28}H_{24}O_{16}$	quercetin-O-galloyl-glucopyranoside
10	1.43	284.0989	284.0987	−0.90	$C_{10}H_{13}N_5O_5$	guanosine	143	11.08	623.1618	623.1622	0.76	$C_{28}H_{32}O_{16}$	isorhamnetin-3-O-nehesperidine
11	1.45	132.1019	132.1019	−0.27	$C_6H_{13}NO_2$	leucine	144	11.12	370.1649	370.1646	−0.94	$C_{21}H_{23}NO_5$	allocryptopine
12	1.48	331.0671	331.0674	1.03	$C_{13}H_{16}O_{10}$	gallic acid-4-O-β-D-glucopyranoside	145*	11.26	515.1195	515.1198	0.49	$C_{25}H_{24}O_{12}$	isochlorogenic acid B
13*	1.49	330.0598	330.0592	−1.72	$C_{10}H_{12}N_5O_6P$	adenosine cyclophosphate	146	11.29	340.1543	340.1540	−1.10	$C_{20}H_{21}NO_4$	papaverine
14	1.51	302.1387	302.1383	−1.24	$C_{17}H_{19}NO_4$	morphine N-oxide	147	11.33	579.1719	579.1726	1.07	$C_{27}H_{32}O_{14}$	naringin
15	1.69	331.0671	331.0674	1.03	$C_{13}H_{16}O_{10}$	gallic acid-3-O-β-D-glucopyranoside	148*	11.42	593.1512	593.1517	0.91	$C_{27}H_{30}O_{15}$	kaempferol-3-O-rutinoside
16	1.80	286.1438	286.1433	−1.61	$C_{17}H_{19}NO_3$	morphine	149	11.44	414.1547	414.1541	−1.57	$C_{22}H_{23}NO_7$	noscapine isomer 1
17*	1.98	169.0142	169.0134	−4.95	$C_7H_6O_5$	gallic acid	150*	11.55	515.1195	515.1201	1.09	$C_{25}H_{24}O_{12}$	1,5-dicaffeoylquinic acid
18	2.44	166.0863	166.0862	−0.27	$C_9H_{11}NO_2$	phenylalanine	151*	11.56	137.0244	137.0235	−7.06	$C_7H_6O_3$	salicylic acid
19	3.23	179.0350	179.0553	−4.81	$C_9H_8O_4$	caffeic acid isomer	152	11.63	623.1981	623.1992	1.73	$C_{29}H_{36}O_{15}$	isoacteoside
20	3.32	197.0455	197.0448	−3.64	$C_9H_{10}O_5$	danshensu	153	11.65	400.1391	400.1387	−1.02	$C_{21}H_{21}NO_7$	narcotoline
21	3.51	329.0878	329.0882	1.29	$C_{14}H_{18}O_9$	pseudolaroside B	154*	11.70	515.1195	515.1199	0.72	$C_{25}H_{24}O_{12}$	isochlorogenic acid A
22	3.75	153.0193	153.0185	−5.76	$C_7H_6O_4$	protocatechuic acid	155	11.73	491.0831	491.0836	0.97	$C_{22}H_{20}O_{13}$	isorhamnetin-7-O-glucuronide
23	3.88	153.0557	153.0548	−5.93	$C_8H_{10}O_3$	3,4-dihydroxyphenylethanol	156	11.73	519.1872	519.1877	1.07	$C_{26}H_{32}O_{11}$	pinoresinol 4-O-β-D-glucopyranoside
24	4.15	451.1246	451.1249	0.78	$C_{21}H_{24}O_{11}$	catechin-5-O-glucoside	157	11.78	577.1563	577.1569	1.11	$C_{27}H_{30}O_{14}$	apigenin-7-O-rutinoside
25	4.16	205.0972	205.0971	−0.07	$C_{11}H_{12}N_2O_2$	tryptophan	158	11.78	623.1618	623.1619	0.18	$C_{28}H_{32}O_{16}$	isorhamnetin-3-O-rutinoside
26	4.25	483.0780	483.0784	0.83	$C_{20}H_{20}O_{14}$	gallic acid-O-galloyl-glucoside	159	11.85	414.1547	414.1541	−1.42	$C_{22}H_{23}NO_7$	noscapine isomer 2
27	4.33	448.1966	448.1965	−0.14	$C_{23}H_{29}NO_8$	N-methylnorcoclaurine-7-O-glucoside	160	11.90	565.1563	565.1571	1.45	$C_{26}H_{30}O_{14}$	hydroxyliquiritin apioside
28	4.33	515.1406	515.1411	0.82	$C_{22}H_{28}O_{14}$	chlorogenic acid-hexoside	161	11.93	447.0933	447.0936	0.64	$C_{21}H_{20}O_{11}$	luteolin-4′-O-glucoside
29	4.43	311.0409	311.0412	1.21	$C_{13}H_{12}O_9$	caftaric acid	162	12.11	446.1809	446.1802	−1.71	$C_{23}H_{27}NO_8$	narceine
30	4.47	272.1281	272.1277	−1.47	$C_{16}H_{17}NO_3$	DL-demethylcoclaurine	163	12.17	282.1489	282.1485	−1.26	$C_{18}H_{19}NO_2$	O-nornuciferine
31*	4.51	353.0878	353.0880	0.67	$C_{16}H_{18}O_9$	neochlorogenic acid	164	12.17	433.1140	433.1143	0.55	$C_{21}H_{22}O_{10}$	naringenin-7-O-glucoside

Table 1 (*continued*)

peak	t_R	Theoretical Mass m/z	Experimental Mass m/z	Error (ppm)	Formula	Identification	peak	t_R	Theoretical Mass m/z	Experimental Mass m/z	Error (ppm)	Formula	Identification
32	4.52	462.2122	462.2115	−1.70	$C_{24}H_{31}NO_8$	N-methylcoclaurine-7-O-glucoside	**165**	12.28	431.0984	431.0985	0.19	$C_{21}H_{20}O_{10}$	emodin-1-O-D-glucoside
33	4.54	300.1594	300.1589	−1.83	$C_{18}H_{21}NO_3$	codeine	**166**	12.36	445.0776	445.0779	0.62	$C_{21}H_{18}O_{11}$	apigenin-7-O-glucuronide
34	4.58	285.0616	285.0619	1.16	$C_{12}H_{14}O_8$	uralenneoside isomer1	**167***	12.37	609.1825	609.1832	1.21	$C_{28}H_{34}O_{15}$	hesperidin
35	4.71	163.0401	163.0392	−5.63	$C_9H_8O_3$	coumaric acid	**168***	12.43	515.1195	515.1197	0.37	$C_{25}H_{24}O_{12}$	isochlorogenic acid C
36	4.80	483.0780	483.0784	0.83	$C_{20}H_{20}O_{14}$	gallic acid-O-galloyl-glucoside	**169**	12.43	607.1668	607.1674	0.95	$C_{28}H_{32}O_{15}$	diosmin
37	4.81	448.1966	448.1962	−0.94	$C_{23}H_{29}NO_8$	N-methylnorcoclaurine-4′-O-glucoside	**170***	12.48	359.0772	359.0772	−0.09	$C_{18}H_{16}O_8$	rosmarinic acid
38	4.89	285.0616	285.0619	1.05	$C_{12}H_{14}O_8$	uralenneoside isomer 2	**171**	12.53	491.0831	491.0834	0.66	$C_{22}H_{20}O_{13}$	isorhamnetin-3-O-glucuronide
39	5.04	451.1246	451.1249	0.72	$C_{21}H_{24}O_{11}$	catechin-7-O-glucoside	**172**	12.56	463.1235	463.1233	−0.49	$C_{22}H_{22}O_{11}$	tectoridin
40	5.21	339.0722	339.0727	1.58	$C_{15}H_{16}O_9$	esculin	**173**	12.66	639.1920	639.1920	0.09	$C_{29}H_{34}O_{16}$	aurantio-obtusin-6-O-rutinoside
41	5.27	137.0244	137.0234	−7.28	$C_7H_6O_3$	4-hydroxybenzoic acid	**174**	12.69	463.1235	463.1231	−0.82	$C_{22}H_{22}O_{11}$	homoplantaginin
42	5.40	483.0780	483.0783	0.58	$C_{20}H_{20}O_{14}$	gallic acid-O-galloyl-glucoside	**175**	12.71	463.1246	463.1250	0.90	$C_{22}H_{24}O_{11}$	hesperetin-7-O-β-D-glucoside
43	5.50	515.1406	515.1412	1.05	$C_{22}H_{28}O_{14}$	chlorogenic acid-hexoside	**176**	12.74	549.1614	549.1621	1.36	$C_{26}H_{30}O_{13}$	licuraside
44	5.63	451.1246	451.1249	0.65	$C_{21}H_{24}O_{11}$	catechin-4′-O-glucoside	**177**	12.79	431.0984	431.0986	0.53	$C_{21}H_{20}O_{10}$	aloe-emodin-3-(hydroxymethyl)-O-β-D-glucopyranoside
45	5.65	483.0780	483.0785	0.96	$C_{20}H_{20}O_{14}$	gallic acid-O-galloyl-glucoside	**178**	12.79	591.1719	591.1727	1.25	$C_{28}H_{32}O_{14}$	liquiritigenin-4′-O-(β-D-3-O-acetyl-apiofuranosyl-(1 → 2)-β-d-glucopyranoside
46	5.71	314.1751	314.1747	−1.15	$C_{19}H_{23}NO_3$	lotusine	**179**	12.80	463.1235	463.1234	−0.10	$C_{22}H_{22}O_{11}$	diosmetin-7-O-β-D-glucopyranoside
47	5.74	337.0929	337.0933	1.27	$C_{16}H_{18}O_8$	5-p-coumaroylquinic acid	**180**	12.85	447.0933	447.0933	0.01	$C_{21}H_{20}O_{11}$	luteolin-3′-O-glucoside
48	5.86	316.1543	316.1540	−1.00	$C_{18}H_{21}NO_4$	norreticuline	**181**	12.86	475.0882	475.0885	0.57	$C_{22}H_{20}O_{12}$	diosmetin-7-O-glucuronide
49	5.92	515.1406	515.1411	0.93	$C_{22}H_{28}O_{14}$	chlorogenic acid-hexoside	**182**	12.89	459.1297	459.1302	1.13	$C_{23}H_{24}O_{10}$	6′-acetylliquiritin
50	6.02	483.0780	483.0786	1.14	$C_{20}H_{20}O_{14}$	gallic acid-O-galloyl-glucoside	**183**	12.90	417.1191	417.1195	0.90	$C_{21}H_{22}O_9$	isoliquiritin
51	6.04	451.1246	451.2189	0.85	$C_{21}H_{24}O_{11}$	catechin-3′-O-glucoside	**184**	12.92	493.1341	493.1340	−0.17	$C_{23}H_{24}O_{12}$	aurantio-obtusin-6-O-glucoside
53*	6.14	353.0878	353.0881	0.75	$C_{16}H_{18}O_9$	chlorogenic acid	**185**	12.96	431.1337	431.1334	−0.69	$C_{22}H_{22}O_9$	ononin
52	6.14	325.0929	325.0931	0.77	$C_{15}H_{18}O_8$	coumaric acid-O-glucoside	**186**	12.99	417.1191	417.1195	0.97	$C_{21}H_{22}O_9$	neoisoliquiritin
54	6.16	635.0890	635.0895	0.78	$C_{27}H_{24}O_{18}$	tri-O-galloyl-glucoside	**187**	13.03	433.0776	433.0779	0.50	$C_{20}H_{18}O_{11}$	quercetin 3-O-arabinoside
55*	6.37	353.0878	353.0881	0.84	$C_{16}H_{18}O_9$	cryptochlorogenic acid	**188**	13.04	695.1981	695.2002	−2.09	$C_{35}H_{36}O_{15}$	licorice-glycoside B
56	6.40	286.1438	286.1436	−0.77	$C_{17}H_{19}NO_3$	coclaurine	**189**	13.09	725.2087	725.2099	1.64	$C_{36}H_{38}O_{16}$	licorice-glycoside A

Table 1 (*continued*)

peak	t_R	Theoretical Mass m/z	Experimental Mass m/z	Error (ppm)	Formula	Identification	peak	t_R	Theoretical Mass m/z	Experimental Mass m/z	Error (ppm)	Formula	Identification
57	6.48	300.1594	300.1592	−0.80	$C_{18}H_{21}NO_3$	N-methylisococlaurine	**190**	13.09	459.0933	459.0938	1.21	$C_{22}H_{20}O_{11}$	carboxyl-chrysophanol-O-glucose
58	6.52	291.0146	291.0148	0.55	$C_{13}H_8O_8$	brervifolincaboxylic acid	**191**	13.21	283.0612	283.0607	−1.76	$C_{16}H_{12}O_5$	glycitein
59	6.55	367.1035	367.1041	1.84	$C_{17}H_{20}O_9$	4-feruloylquinic acid	**192**	13.21	447.0933	447.0935	0.44	$C_{21}H_{20}O_{11}$	isorhamnetin-3-O-arabinoside
60	6.63	483.0780	483.0785	0.96	$C_{20}H_{20}O_{14}$	gallic acid-O-galloyl-glucoside	**193**	13.25	593.1876	593.1881	0.90	$C_{28}H_{34}O_{14}$	didymin
61	6.63	625.1410	625.1420	1.61	$C_{27}H_{30}O_{17}$	quercetin-3-O-diglucoside	**194**	13.27	255.0663	255.0663	0.19	$C_{15}H_{12}O_4$	liquiritigenin
62	6.67	325.0929	325.0933	1.14	$C_{15}H_{18}O_8$	coumaric acid-O-glucoside	**195**	13.27	373.0929	373.0931	0.59	$C_{19}H_{18}O_8$	methyl rosmarinate
63	6.67	635.0890	635.0898	1.34	$C_{27}H_{24}O_{18}$	tri-O-galloyl-glucoside	**196**	13.29	473.1089	473.1090	0.16	$C_{23}H_{22}O_{11}$	aloe-emodin-8-O-(6-O-acetyl)-glucoside
64	6.67	771.1989	771.2005	2.03	$C_{33}H_{40}O_{21}$	quercetin-3-O-sophoroside-7-O-rhamnoside	**197**	13.31	999.4442	999.4453	1.00	$C_{48}H_{72}O_{22}$	24-hydroxy-licoricesaponin A3
65*	6.71	179.0350	179.0343	−3.87	$C_9H_8O_4$	caffeic acid	**198**	13.35	837.3914	837.3927	1.52	$C_{42}H_{62}O_{17}$	yunganoside K2
66	6.76	635.0890	635.0897	1.06	$C_{27}H_{24}O_{18}$	tri-O-galloyl-glucoside	**199**	13.40	489.1038	489.1059	4.25	$C_{23}H_{22}O_{12}$	luteolin-7-O-6″-ocetylglucoside
67	6.81	328.1543	328.1541	−0.87	$C_{19}H_{21}NO_4$	boldine	**200**	13.41	407.1348	407.1350	0.48	$C_{20}H_{24}O_9$	torachrysone-8-O-glucoside
68	6.82	344.1856 $[M]^+$	344.1853	−0.88	$C_{20}H_{26}NO_4^+$	N-methylreticuline	**201***	13.42	285.0405	285.0406	0.45	$C_{15}H_{10}O_6$	luteolin
69	6.85	579.1719	579.1729	1.59	$C_{27}H_{32}O_{14}$	liquiritigenin-O-diglucuronide	**202**	13.42	431.0984	431.0985	0.26	$C_{21}H_{20}O_{10}$	emodin-8-O-D-glucoside
70	7.09	386.1598	386.1597	−0.37	$C_{21}H_{23}NO_6$	glaucamine	**203***	13.44	301.0354	301.0356	0.78	$C_{15}H_{10}O_7$	quercetin
71	7.09	711.2141	711.2150	1.10	$C_{32}H_{40}O_{18}$	glucoliquirtin asioside	**204**	13.45	415.1035	415.1037	0.66	$C_{21}H_{20}O_9$	chrysophanol-1-O-β-D-glucoside
72*	7.11	342.1699 $[M]^+$	342.1694	−1.62	$C_{20}H_{24}NO_4^+$	magnoflorine	**205**	13.45	253.0506	253.0505	−0.48	$C_{15}H_{10}O_4$	chrysophanol
73	7.15	515.1194	515.1196	0.25	$C_{25}H_{24}O_{12}$	dicaffeylquinic acid	**206**	13.46	447.1286	447.1282	−0.77	$C_{22}H_{22}O_{10}$	calycosin-7-O-β-D-glucoside
74	7.16	314.1750 $[M]^+$	314.1748	−0.86	$C_{19}H_{24}NO_3^+$	isolotusine	**207**	13.46	983.4493	983.4506	1.25	$C_{48}H_{72}O_{21}$	licoricesaponin A3
75	7.17	337.0928	337.0931	0.56	$C_{16}H_{18}O_8$	3-p-coumaroylquinic acid	**208***	13.48	283.0612	283.0611	−0.34	$C_{16}H_{12}O_5$	physcion
76	7.19	325.0928	325.0932	0.95	$C_{15}H_{18}O_8$	coumaric acid-O-glucoside	**209**	13.50	853.3863	853.3876	1.44	$C_{42}H_{62}O_{18}$	22-hydroxy-licoricesaponin G2 isomer 1
77	7.24	328.1543	328.1541	−0.59	$C_{19}H_{21}NO_4$	corytuberine	**210**	13.52	315.0510	315.0513	0.97	$C_{16}H_{12}O_7$	isorhamnetin isomer
78	7.42	153.1273	153.1273	−0.80	$C_{10}H_{16}O$	camphor	**211**	13.52	895.3969	895.3982	1.44	$C_{44}H_{64}O_{19}$	hydroxy acetoxyglycyrrhizin
79	7.42	330.1699	330.1696	−1.29	$C_{19}H_{23}NO_4$	reticuline	**212**	13.53	415.1035	415.1037	0.59	$C_{21}H_{20}O_9$	chrysophanol-8-O-glucoside
80	7.46	300.1594	300.1592	−0.70	$C_{18}H_{21}NO_3$	N-methylcoclaurine	**213**	13.62	301.0707	301.0704	−0.88	$C_{16}H_{12}O_6$	tectorigenin
81	7.48	635.0889	635.0896	0.97	$C_{27}H_{24}O_{18}$	tri-O-galloyl-glucoside	**214**	13.64	315.0510	315.0515	1.35	$C_{16}H_{12}O_7$	isorhamnetin isomer

Table 1 (*continued*)

peak	t_R	Theoretical Mass m/z	Experimental Mass m/z	Error (ppm)	Formula	Identification	peak	t_R	Theoretical Mass m/z	Experimental Mass m/z	Error (ppm)	Formula	Identification
82	7.55	337.0928	337.0932	0.92	$C_{16}H_{18}O_8$	4-p-coumaroylquinic acid	215	13.64	853.3863	853.3878	1.74	$C_{42}H_{62}O_{18}$	22-hydroxy-licoricesaponin G2 isomer 2
83	7.58	593.1511	593.1517	0.91	$C_{27}H_{30}O_{15}$	vicenin II	216	13.70	879.4020	879.4031	1.24	$C_{44}H_{64}O_{18}$	acetoxy-glycyrrhizic acid
84	7.64	635.0889	635.0895	0.78	$C_{27}H_{24}O_{18}$	tri-O-galloyl-glucoside	217	13.72	837.3914	837.3924	1.17	$C_{42}H_{62}O_{17}$	licoricesaponin P2
85	7.67	314.1750	314.1746	−1.43	$C_{19}H_{23}NO_3$	4′-methyl-N-methylcoclaurine	218	13.72	859.3758	859.3742	−1.82	$C_{44}H_{60}O_{17}$	methyllicorice-saponin Q2 isomer 1
86	7.67	314.1750 [M]$^+$	314.1746	−1.43	$C_{19}H_{24}NO_3^+$	magnocurarine	219	13.77	445.1140	445.1145	1.15	$C_{22}H_{22}O_{10}$	physcion-8-O-β-D-glucoside
87	7.67	639.1567	639.1574	1.06	$C_{28}H_{32}O_{17}$	isorhamnetin-3,7-O-diglucoside	220	13.78	329.0667	329.0671	1.32	$C_{17}H_{14}O_7$	jaceosidin
88	7.98	328.1543	328.1541	−0.87	$C_{19}H_{21}NO_4$	scoulerine	221*	13.86	271.0612	271.0614	0.75	$C_{15}H_{12}O_5$	naringenin
89	8.02	298.1438	298.1436	−0.74	$C_{18}H_{19}NO_3$	codeinone	222	13.86	835.3758	835.3762	0.46	$C_{42}H_{60}O_{17}$	yunganoside M
90	8.08	635.0890	635.0898	1.25	$C_{27}H_{24}O_{18}$	tri-O-galloyl-glucoside	223	13.89	283.0612	283.0613	0.51	$C_{16}H_{12}O_5$	acacetin
91	8.39	356.1492	356.1489	−0.98	$C_{20}H_{21}NO_5$	amurensinine N-oxide A	224	13.89	445.1140	445.1144	0.94	$C_{22}H_{22}O_{10}$	physcion-1-O-β-D-glucoside
92	8.39	367.1035	367.1045	2.90	$C_{17}H_{20}O_9$	5-feruloylquinic acid	225	13.91	269.0455	269.0457	0.64	$C_{15}H_{10}O_5$	apigenin
93	8.43	635.0890	635.0886	−0.58	$C_{27}H_{24}O_{18}$	tri-O-galloyl-glucoside	226	13.93	329.0667	329.0669	0.56	$C_{17}H_{14}O_7$	iristectorigenin B
94	8.45	300.1594	300.1591	−1.20	$C_{18}H_{21}NO_3$	6-demethyl-4′-methyl-N-methylcoclaurine	227	13.98	879.4020	879.4040	−1.72	$C_{44}H_{64}O_{18}$	acetoxy-glycyrrhizic acid
95	8.45	344.1856	344.1852	−1.23	$C_{20}H_{25}NO_4$	codamine	228*	13.99	285.0405	285.0407	0.87	$C_{15}H_{10}O_6$	kaempferol
96	8.60	268.1332	268.1329	−1.03	$C_{17}H_{17}NO_2$	caaverine	229	14.10	301.0707	301.0702	−1.68	$C_{16}H_{12}O_6$	hispidulin
97	8.60	337.0929	337.0935	1.75	$C_{16}H_{18}O_8$	1-p-coumaroylquinic acid	230	14.10	301.0718	301.0721	1.16	$C_{16}H_{14}O_6$	hesperetin
98	8.62	625.1410	625.1417	1.12	$C_{27}H_{30}O_{17}$	myricetin-3-O-rutinoside	231	14.11	819.3809	819.3823	1.78	$C_{42}H_{60}O_{16}$	licoricesaponin E2
99*	8.63	163.0401	163.0392	−5.20	$C_9H_8O_3$	4-coumaric acid	232	14.11	837.3914	837.3922	0.94	$C_{42}H_{62}O_{17}$	licoricesaponin Q2
100	8.67	579.1719	579.1727	1.28	$C_{27}H_{32}O_{14}$	liquiritigenin-O-diglucuronide	233	14.11	859.3758	859.3737	−2.39	$C_{44}H_{60}O_{17}$	methyllicorice-saponin Q2 isomer 2
101	8.68	563.1406	563.1412	0.96	$C_{26}H_{28}O_{14}$	schaftoside	234	14.11	967.4544	967.4556	1.19	$C_{48}H_{72}O_{20}$	haoglycyrrhizin isomer 1
102	8.83	459.0933	459.0937	0.94	$C_{22}H_{20}O_{11}$	carboxyl-chrysophanol-O-glucose	235*	14.14	315.0510	315.0514	1.16	$C_{16}H_{12}O_7$	isorhamnetin
103	8.84	625.1410	625.1417	1.12	$C_{27}H_{30}O_{17}$	quercetin-7-O-diglucoside	236	14.22	301.0707	301.0705	−0.65	$C_{16}H_{12}O_6$	diosmetin
104	8.87	344.1856	344.1853	−0.97	$C_{20}H_{25}NO_4$	laudanine	237	14.22	837.3914	837.3923	1.08	$C_{42}H_{62}O_{17}$	uralsaponin N
105	8.89	312.1594	312.1589	−1.54	$C_{19}H_{21}NO_3$	thebaine	238	14.24	863.4071	863.4081	1.17	$C_{44}H_{64}O_{17}$	acetoxyglycyrrhaldehyde
106	8.91	326.1387	326.1382	−1.45	$C_{19}H_{19}NO_4$	pacodine (7-O-demethylpapaverine)	239	14.27	449.1453	449.1456	0.69	$C_{22}H_{26}O_{10}$	torachrysone-O-acetylglucoside
107	8.96	367.1035	367.1043	2.24	$C_{17}H_{20}O_9$	3-feruloylquinic acid	240	14.35	255.0663	255.0661	−0.64	$C_{15}H_{12}O_4$	isoliquiritigenin
108	9.08	463.0882	463.0887	0.97	$C_{21}H_{20}O_{12}$	quercetin-5-O-glucoside	242*	14.36	821.3965	821.3973	0.94	$C_{42}H_{62}O_{16}$	glycyrrhizic acid
109	9.36	433.1140	433.1143	0.55	$C_{21}H_{22}O_{10}$	naringenin-4′-O-glucoside	241	14.36	329.0667	329.0668	0.47	$C_{17}H_{14}O_7$	aurantio-obtusin
110	9.37	314.1751	314.1749	−0.45	$C_{19}H_{23}NO_3$	armepavine	243	14.38	837.3914	837.3920	0.72	$C_{42}H_{62}O_{17}$	hydroxyglycyrrhizin
111	9.40	417.1180	417.1178	−0.43	$C_{21}H_{20}O_9$	daidzin	244	14.48	457.1140	457.1146	1.18	$C_{23}H_{22}O_{10}$	chrysophanol-O-

Table 1 (*continued*)

peak	t_R	Theoretical Mass m/z	Experimental Mass m/z	Error (ppm)	Formula	Identification	peak	t_R	Theoretical Mass m/z	Experimental Mass m/z	Error (ppm)	Formula	Identification
112	9.41	342.1700	342.1698	−0.45	$C_{20}H_{23}NO_4$	tetrahydrocolumbamine	**245**	14.55	354.1336	354.1335	−0.17	$C_{20}H_{19}NO_5$	acetylglucoside pseudoprotopine
113	9.59	579.1719	579.1726	1.07	$C_{27}H_{32}O_{14}$	liquiritigenin-O-diglucuronide	**246**	14.55	967.4544	967.4561	1.76	$C_{48}H_{72}O_{20}$	haoglycyrrhizin isomer 2
114	9.59	621.1097	621.1104	1.01	$C_{27}H_{26}O_{17}$	apigenin-7-O-diglucuronide	**247**	14.60	837.3914	837.3924	1.17	$C_{42}H_{62}O_{17}$	hydroxyglycyrrhizin
115	9.63	326.1387	326.1384	−0.87	$C_{19}H_{19}NO_4$	palaudine (3′-O-demethylpapaverine)	**248**	14.73	821.3965	821.3975	1.23	$C_{42}H_{62}O_{16}$	licoricesaponin H2
116	9.67	549.1614	549.1619	1.03	$C_{26}H_{30}O_{13}$	liquiritin apioside	**249**	14.76	807.4172	807.4185	1.51	$C_{42}H_{64}O_{15}$	licoricesaponin B2
117	9.69	595.1668	595.1679	1.79	$C_{27}H_{32}O_{15}$	eriocitrin	**250**	14.80	955.4908	955.4923	1.58	$C_{48}H_{76}O_{19}$	yunganoside C1
118	9.72	417.1191	417.1195	0.83	$C_{21}H_{22}O_9$	neoliquiritin	**251**	14.82	369.1333	369.1329	−1.07	$C_{21}H_{20}O_6$	gancaonin N
119	9.81	433.1140	433.1144	0.97	$C_{21}H_{22}O_{10}$	naringenin-5-O-glucoside	**252**	14.94	955.4908	955.4924	1.70	$C_{48}H_{76}O_{19}$	yunganoside A1
120	9.94	428.1704	428.1699	−1.21	$C_{23}H_{25}NO_7$	N-methylnarcotine	**253**	15.03	479.2650	479.2654	0.83	$C_{26}H_{40}O_8$	steviol-19-O-glucoside
121	9.95	549.1614	549.1617	0.69	$C_{26}H_{30}O_{13}$	isoliquiritin apioside	**254**	15.10	297.0405	297.0406	0.33	$C_{16}H_{10}O_6$	6-methyl-rhein
122	9.97	517.0412	517.0438	4.86	$C_{26}H_{14}O_{12}$	1,1,3,4,5,6,8,8′-octahydroxy-9H,9′H-2,2′-bixanthene-9,9′-dione	**255**	15.17	953.4752	953.4742	−0.96	$C_{48}H_{74}O_{19}$	yunganoside D1
123	9.98	417.1191	417.1193	0.51	$C_{21}H_{22}O_9$	liquiritin	**256***	15.44	283.0248	283.0249	0.31	$C_{15}H_8O_6$	rheic acid
124	10.00	370.1649	370.1643	−1.75	$C_{21}H_{23}NO_5$	cryptopine	**257**	15.54	343.0823	343.0825	0.57	$C_{18}H_{16}O_7$	eupatilin
125*	10.01	609.1461	609.1467	1.02	$C_{27}H_{30}O_{16}$	rutin	**258**	15.67	283.0612	283.0613	0.40	$C_{16}H_{12}O_5$	biochanin A
126	10.03	537.1038	537.1040	0.28	$C_{27}H_{22}O_{12}$	lithospermic acid isomer	**259**	15.72	369.1333	369.1329	−1.07	$C_{21}H_{20}O_6$	glicoricone
127	10.06	354.1336	354.1336	−0.05	$C_{20}H_{19}NO_5$	protopine	**260**	15.72	807.4172	807.4184	1.43	$C_{42}H_{64}O_{15}$	22-dehydrouralsaponin C
128*	10.09	300.9990	300.9991	0.40	$C_{14}H_6O_8$	ellagic acid	**261**	15.83	355.1187	355.1193	1.63	$C_{20}H_{20}O_6$	uralenin
129	10.10	431.0984	431.0985	0.33	$C_{21}H_{20}O_{10}$	apigenin-7-O-β-D-glucoside	**262**	15.98	589.1351	589.1359	1.21	$C_{31}H_{26}O_{12}$	1-methyl-8-hydroxy-9,10-anthraquinone-3-O-(6′-O-cinnamoyl)-glucoside
130	10.12	358.2013	358.2008	−1.24	$C_{21}H_{27}NO_4$	laudanosine	**263***	16.27	593.1301	593.1309	1.34	$C_{30}H_{26}O_{13}$	procyanidin
131*	10.23	463.0882	463.0888	1.32	$C_{21}H_{20}O_{12}$	hyperoside	**264***	17.72	269.0455	269.0458	0.87	$C_{15}H_{10}O_5$	emodin
132	10.29	593.1512	593.1520	1.43	$C_{27}H_{30}O_{15}$	luteolin-7-O-rutinoside	**265***	23.15	469.3323	469.3333	1.95	$C_{30}H_{46}O_4$	18 β-glycyrrhetintic acid
133	10.34	344.1856	344.1855	−0.51	$C_{20}H_{25}NO_4$	tetrahydropapaverine							

* Compared with standard compounds.
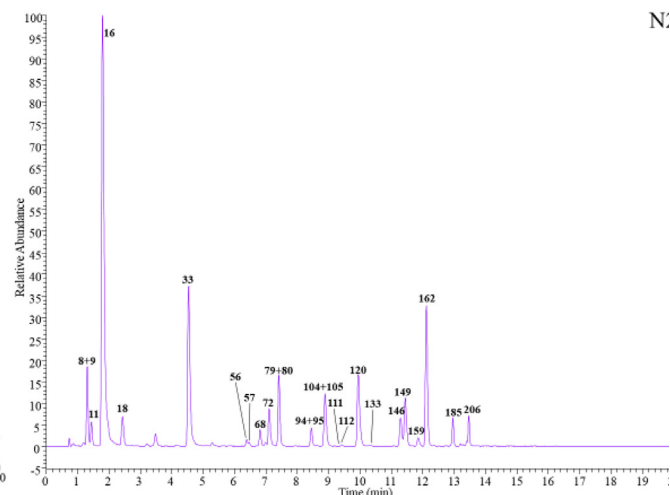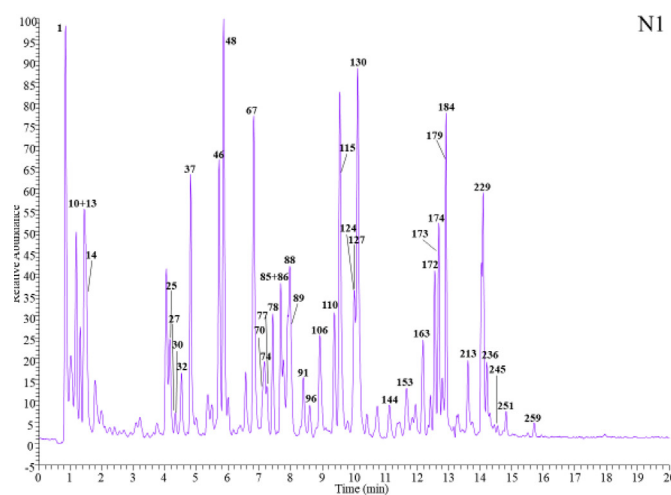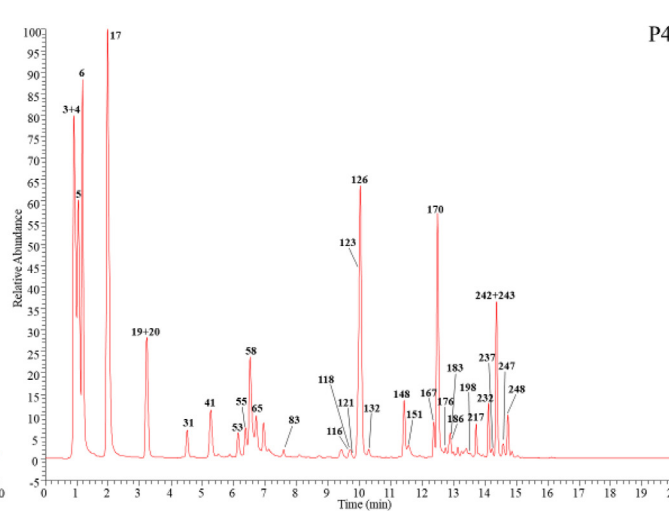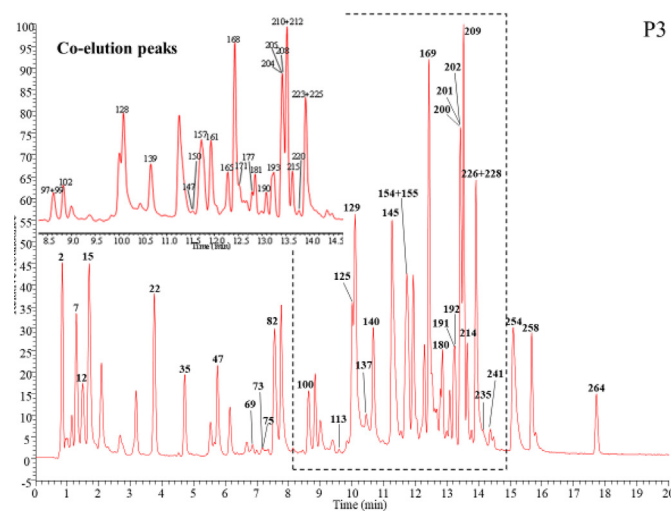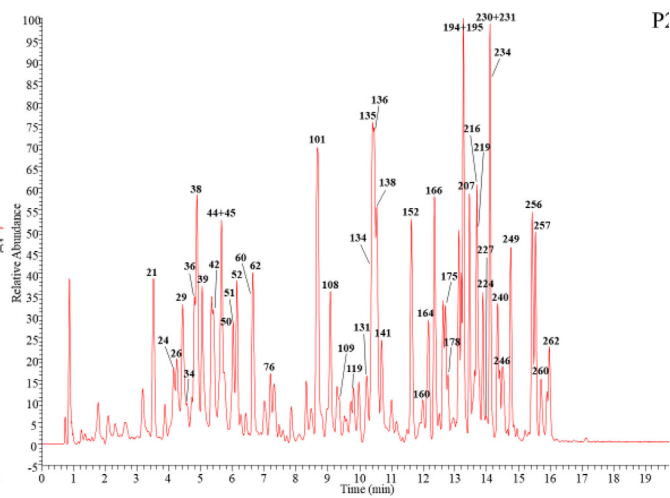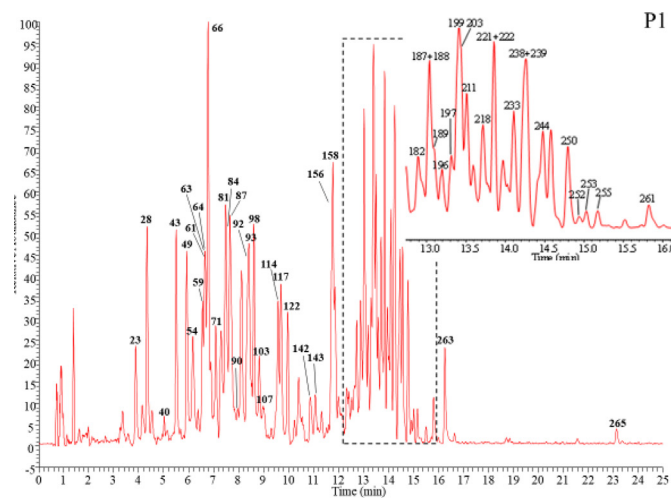
$[C_{10}H_{12}O_2N]^+$ and 151.075 $[C_9H_{11}O_2]^+$ due to RDA fragmentation and cleavage of the B-ring, respectively. Another characteristic ion at m/z 163.060 was indicated by the loss of the methyl radical from the ion at m/z 178.086 (Jeong et al., 2012).

3.1.1.2. Identification of aporphine alkaloids. For aporphine alkaloids, the elimination of CH_3NR group as well as lose CH_3OH moiety and CO were the characteristic fragmentation patterns. Peak **72** showed precursor ion $[M]^+$ at m/z 342.1699, which produced characteristic ions at m/z 297.111 $[M-(CH_3)_2NH]^+$, 282.088 $[M-(CH_3)_2NH-CH_3]^+$, 265.085 $[M-(CH_3)_2NH-CH_3OH]^+$. Comparing with reference standards, peak **72** was accurately identified as magnoflorine. Similarly, peaks **67**, **77** were pairs of isomers with $[M + H]^+$ ion at m/z 328.1543 and exhibited three major diagnostic fragment ions at m/z 297.111 $[M + H-CH_3NH_2]^+$, 265.085 $[M + H-CH_3NH_2-CH_3OH]^+$, 237.090 $[M + H-CH_3NH_2-CH_3OH-CO]^+$. Therefore, peaks **67**, **77** were respectively determined as boldine and corytuberine according to their retention behavior on the chromatographic column (Conceição et al., 2020). Similarly, peaks **96** and **163** were considered as caaverine and O-nornuciferine.

3.1.1.3. Identification of benzyltetrahydroisoquinoline alkaloids. For benzyltetrahydroisoquinoline alkaloids, they were easy to observe the elimination of NRH_2, CH_3OH groups and other characteristic ions at m/z 175.075 $[C_{11}H_{11}O_2]^+$, 161.059 $[C_{10}H_9O_2]^+$, 121.064 $[C_8H_9O]^+$, 107.049 $[C_7H_7O]^+$. Peak **30** with the parent ion $[M + H]^+$ at m/z 272.12811, was easy to produce fragment ions at m/z 255.101 $[M + H-NH_3]^+$, 161.059 $[M + H-NH_3-C_6H_5O]^+$, and 107.049 $[M + H-C_9H_{11}N_2O]^+$. Consequently, it was tentatively determined to be DL-demethylcoclaurine based on the related literature (Oh et al., 2018). Peak **56** showed the $[M + H]^+$ ion at m/z 286.1437, which yielded characteristic ions at m/z 269.117 $[M + H-NH_3]^+$, 237.090 $[M + H-NH_3-CH_3OH]^+$, 175.075 $[M + H-NH_3-C_6H_6O]^+$, so peak **56** was tentatively named coclaurine (Menéndez-Perdomo et al., 2021). Similarly, peaks **27**, **32**, **37**, **46**, **57**, **74**, **80**, **85**, **86**, **94**, **110** were successfully identified as N-methylnorcoclaurine-7-O-glucoside, N-methylcoclaurine-7-O-glucoside, N-methylnorcoclaurine-4'-O-glucoside, lotusine, N-methylisococlaurine, isolotusine, N-methylcoclaurine, 4'-methyl-N-methylcoclaurine, magnocu-

rarine, 6-demethyl-4'-methyl-N-methylcoclaurine, armepavine. Peak 130 had a retention time of 10.12 min and the $[M]^+$ ion at m/z 358.2012. The fragmentation ions at m/z 327.158 $[M + H-CH_3NH_2]^+$, 206.117 $[C_{12}H_{16}NO_2]^+$, 189.090 $[C_{12}H_{16}NO_2-NH_3]^+$, and 151.075$[C_9H_{11}O_2]^+$ suggested that peak **130** was tentatively inferred to be laudanosine. On the basis of this method, peaks **48**, **79**, **68**, **95**, **104**, **133** were deduced to be norreticuline, reticuline, N-methylreticuline, codamine, laudanine, tetrahydropapaverine.

3.1.1.4. Identification of phthalideisoquinoline alkaloids. For phthalideisoquinolines, the fragment ions were obtained by the isoquinone after bond cleavage with the phthalide ring as well as the elimination of H_2O and OCH_3 groups (Menéndez-Perdomo et al., 2021). Peak **153** showed a protonated adduct ion at m/z 400.1390 $[M + H]^+$, which fragmented to $[M + H-C_{10}H_{10}O_4]^+$ at m/z 206.081, $[M + H-H_2O]^+$ at m/z 382.127 and $[M + H-H_2O-OCH_3]^+$ at m/z 351.110. Therefore, peak **153** could be considered as narcotoline (Menéndez-Perdomo et al., 2021). Similarly, peaks **120**, **149**, **159**, **162** were identified as N-methylnarcotine, noscapine isomer 1, noscapine isomer 2, narceine.

3.1.1.5. Identification of protopine alkaloids. For protopines, it produced characteristic ions by RDA fragmentation, and subsequent loss of water from the isoquinoline fragment (Jeong et al., 2012). Peak **144** showed the parent ion at m/z 370.1648 $[M + H]^+$, and fragment ions at m/z 352.154 $[M + H-H_2O]^+$, 206.081 $[C_{11}H_{12}NO_3]^+$, and 188.070 $[C_{11}H_{12}NO_3-H_2O]^+$. Then, peak **144** was characterized as allocryptopine based on the Orbitrap Traditional Chinese Medicine Library (OTCML). Likewise, peaks **70**, **91**, **124**, **127**, **245** were assigned as glaucamine, amurensinine N-oxide A, cryptopine, protopine, pseudoprotopine according to the OTCML database and relevant literature (Oh et al., 2018).

3.1.1.6. Identification of morphinan alkaloids. Peak **16** exhibited a protonated molecular ion at m/z 286.1437 $[M + H]^+$, which fragmented to $[M + H-CH_2CHNHCH_3-CO]^+$ at m/z 201.090 and $[M + H-CH_2CHNHCH_3-H_2O]^+$ at m/z 211.075. Therefore, this information led to the tentative conclusion that peak **16** was identified as morphine (Menéndez-Perdomo et al., 2021). Peak **33** with $[M + H]^+$ ion at m/z 300.1594, was

Fig. 2 The high resolution extracted ion chromatograms (EICs) of ZKMG in the positive (P) and negative ion mode (N). P1. m/z 153.0557, 271.0611, 301.0353, 339.0721, 355.1187, 367.1034, 433.0776, 449.1453, 457.1140, 459.1296, 469.3323, 473.1089, 479.2650, 489.1038, 515.1406, 517.0412, 519.1871, 593.1300, 595.1668, 615.0991, 621.1097, 623.1617, 625.1410, 635.0889, 639.1566, 695.1981, 711.2141, 725.2087, 771.1989, 835.3757, 859.3757, 863.4070, 895.3969, 953.4751, 955.4908, 999.4442; P2. m/z 255.0662, 283.0248, 285.0615, 301.0717, 311.0408, 325.0928, 329.0878, 343.0823, 373.0928, 433.1140, 445.0776, 445.1140, 451.1245, 463.0881, 463.1245, 477.0674, 483.0780, 563.1406, 565.1562, 589.1351, 591.1719, 623.1981, 807.4172, 819.3808, 879.4019, 967.4544, 983.4493; P3. m/z 153.0193, 163.0400, 191.0561, 253.0506, 269.0455, 283.0611, 285.0404, 297.0404, 300.9989, 315.0510, 329.0666, 331.0670, 337.0928, 407.1347, 415.1034, 431.0983, 447.0932, 459.0932, 461.0725, 475.0881, 491.0831, 515.1194, 577.1562, 579.1719, 593.1875, 607.1668, 609.1461, 853.3863; P4. m/z 133.0142, 137.0244, 169.0142, 179.0349, 191.0197, 197.0455, 291.0146, 353.0878, 359.0772, 417.1191, 537.1038, 549.1613, 593.1511, 609.1824, 821.3965, 837.3914; N1. m/z136.0617, 153.1273, 205.0971, 268.1332, 272.1281, 282.1488, 284.0989, 298.1437, 301.0706, 302.1386, 314.1750, 314.1761, 316.1543, 326.1386, 328.1543, 330.0597, 354.1335, 356.1492, 358.2012, 369.1332, 370.1648, 386.1598, 400.1390, 448.1965, 462.2122, 463.1234, 493.1340, 639.1919; N2. m/z 132.1019, 166.0862, 268.1040, 286.1437, 300.1594, 312.1594, 330.1699, 340.1543, 342.1699, 344.1856, 414.1547, 417.1180, 428.1703, 431.1336, 446.1809, 447.1285.

14.015 Da (CH_2) higher than the mass of the $[M + H]^+$ ion of peak **16** and generated fragment ions at m/z 215.106 $[M + H-CH_2CHNHCH_3-CO]^+$, 225.090 $[M + H-CH_2CHNHCH_3-H_2O]^+$. Peak **33** was characterized as codeine (Menéndez-Perdomo et al., 2021). Moreover, peaks **14**, **89**, **105** were respectively considered as morphine N-oxide, codeinone and thebaine (Oh et al., 2018; Menéndez-Perdomo et al., 2021).

3.1.1.7. Identification of benzylisoquinoline alkaloids. The precursor ion of peak **146** at m/z 340.1543 and the fragment ions at m/z 202.085 $[C_{12}H_{12}O_2N]^+$ and 324.122 $[M + H-CH_4]^+$ were formed by rearrangement of the C3′ and C4′ methoxy groups to a methylenedioxy bridge. Hence, peak **146** was identified as papaverine (Menéndez-Perdomo et al., 2021). Similarly, peaks **106**, **115** were considered as pacodine and palaudine, respectively.

3.1.2. Identification of flavonoids

Flavonoids usually consist of the framework C6-C3-C6 that are formed when two phenyl rings (A and B) bind with C3, most of them undergo RDA cleavage (Luo et al., 2019). Totally, 92 flavonoids were characterized including 7 chalcones, 5 flavan-3-ols, 24 flavones, 25 flavonols, 21 flavonones, and 10 isoflavones in ZKMG. The proposed fragmentation pathways of each-type representative flavonoids (peaks **183**, **24**, **129**, **235**, **221**, **213**) were observed in Supplementary Figure S2.

3.1.2.1. Identification of chalcone flavonoids. The chalcones (1,3-diaryl-2-propen-1-ones) mainly derived from GU, which are open chain flavonoids. Peaks **183** and **186** showed the same $[M-H]^-$ ion at m/z 417.1191, which further yielded fragment ions at m/z 255.066 $[M-H-C_6H_{10}O_5]^-$ by the elimination of glucosyl group, 135.007 $[C_7H_3O_3]^-$ and 119.048 $[C_8H_7O]^-$ obtained due to RDA cleavage of the C-ring. Based on literature, peaks **183** and **186** were respectively identified as isoliquiritin and neoisoliquiritin (Xue et al., 2021). Peak **240** exhibited $[M-H]^-$ ion at m/z 255.0662, which generated characteristic ions at m/z 135.007 $[C_7H_3O_3]^-$ and 91.017 $[C_7H_3O_3-CO_2]^-$, so it was deduced as isoliquiritigenin based on OTCML database. Similarly, peaks **121**, **176**, **188**, **189** were identified as lsoliquiritin apioside, licuraside, licorice-glycoside B, licorice-glycoside A according to the OTCML database and literature (Xue et al., 2021).

3.1.2.2. Identification of flavan-3-ol flavonoids. Peaks **24**, **39**, **44**, **51** eluted at different time with the same precursor ion $[M-H]^-$ at m/z 451.1245, and the MS^2 spectrum showed fragment ions at m/z 289.072 $[M-H-C_6H_{10}O_5]^-$ by a loss of glucose, 245.081 $[M-H-C_6H_{10}O_5-CO_2]^-$, 137.023 $[M-H-C_6H_{10}O_5-C_8H_8-O_3]^-$. Thus, peaks **24**, **39**, **44**, **51** were tentatively identified as catechin-5-O-glucoside, catechin-7-O-glucoside, catechin-4′-O-glucoside, catechin-3′-O-glucoside based on ClogP values. Peak **263** was unambiguously identified as procyanidin in accordance with the reference standard by comparing with retention time and MS/MS fragmentations.

3.1.2.3. Identification of flavone flavonoids. Peak **225** displayed the protonated molecule ion $[M-H]^-$ at m/z 269.0455, which subsequent fragment ions at m/z 227.034 $[M-H-C_2H_2O]^-$, 225.055 $[M-H-CO_2]^-$, 201.055 $[M-H-C_3O_2]^-$, and 151.002 $[C_7H_3O_4]^-$ due to RDA cleavage, so peak **225** was assigned as apigenin based on OTCML database. Peak **129** exhibited molecular ion $[M-H]^-$ at m/z 431.0983 and the main fragment ion at m/z 269.045 $[M-H-C_6H_{10}O_5]^-$, which indicated peak **225** as aglycone of peak **129**. Therefore, peak **129** was tentatively identified as apigenin-7-O-β-D-glucoside. Likewise, peaks **114**, **157**, **166** were tentatively characterized as apigenin-7-O-diglucuronide, apigenin 7-O-rutinoside, apigenin-7-O-glucuronide. Peak **201** showed $[M-H]^-$ ion at m/z 285.0404, and it could form the fragment ions m/z 241.049 $[M-H-CO_2]^-$, 217.049 $[M-H-C_3O_2]^-$, 199.039 $[M-H-C_2H_2O-CO_2]^-$, 243.029 $[M-H-C_2H_2O]^-$, 175.039 $[M-H-C_2H_2O-C_3O_2]^-$, 133.028 $[C_8H_5O_2]^-$ and 151.002 $[C_7H_3O_4]^-$ due to RDA cleavage. Thus, peak **201** was accurately identified as luteolin by comparing with the reference standard. Peaks **137**, **139**, **161**, **180** displayed the same precursor ion $[M-H]^-$ at m/z 447.0932, which produced the fragment ion at m/z 285.040 $[M-H-C_6H_{10}O_5]^-$. Based on the standard and literature, peaks **137**, **139**, **161**, **180** were respectively assigned as luteolin-5-O-glucoside, cymaroside, luteolin-4′-O-glucoside, luteolin-3′-O-glucoside (Zhao et al., 2019). Similarly, peaks **83**, **199**, **132**, **101**, **261**, **236**, **181**, **179**, **169**, **257**, **229**, **174**, **220**, **223** were tentatively characterized as vicenin II, luteolin-7-O-6″-ocetylglucoside, luteolin-7-O-rutinoside, schaftoside, uralenin, diosmetin, diosmetin-7-O-glucuronide, diosmetin-7-O-β-D-glucopyranoside, diosmin, eupatilin, hispidulin, homoplantaginin, jaceosidin, acacetin based on OTCML database.

3.1.2.4. Identification of flavonol flavonoids. Peak **235** exhibited $[M-H]^-$ ion at m/z 315.0510, yielded fragment ions at m/z 300.027 $[M-H-CH_3]^-$, 271.024 $[M-H-CH_3-CHO]^-$ and 151.002 $[C_7H_3O_4]^-$ by RDA cleavage. Therefore, peak **235** was identified as isorhamnetin according to the retention time of isorhamnetin reference standard and the comparison with MS^2 fragment ions. The protonated molecular ion $[M-H]^-$ of peaks **155** and **171** was m/z 491.0831, which could form MS^2 fragments at m/z 315.051 $[M-H-C_6H_8O_6]^-$ by loss of glucuronide unit and subsequent loss of CH_3 at m/z 300.027 $[M-H-C_6H_8O_6-CH_3]^-$, so they were respectively assigned as isorhamnetin-7-O-glucuronide and isorhamnetin-3-O-glucuronide by comparing with their structures and chromatographic elution order (Nakamura et al., 2018). Correspondingly, peaks **87**, **143**, **158**, **192**, **210**, **214** were respectively characterized as isorhamnetin-3,7-O-diglucoside, isorhamnetin-3-O-nehesperidine, isorhamnetin-3-O-rutinoside, isorhamnetin-3-O-arabinoside, isorhamnetin isomer, isorhamnetin isomer. Peak **203** displayed deprotonated molecular ion $[M-H]^-$ at m/z 301.0353, which produced characteristic ions at m/z 151.002 $[C_7H_3O_4]^-$, 178.997 $[C_8H_3O_5]^-$ due to RDA cleavage. Based on reference standard and MS^2 data, peak **203** was identified as quercetin. Likewise, peaks **61**, **64**, **98**, **103**, **108**, **125**, **131**, **134**, **135**, **136**, **140**, **142**, **148**, **187**, **228** were respectively identified as quercetin-3-O-diglucoside, quercetin-3-O-sophoroside-7-O-rhamnoside, myricetin-3-O-rutinoside, quercetin-7-O-diglucoside, quercetin-5-O-glucoside, rutin, hyperoside, quercetin-7-O-glucoside, quercetin-3-O-glucuronide, isoquercitrin, kaempferol-3-O-β-D-glucuronide, quercetin-O-galloyl-glucopyranoside, kaempferol-3-O-rutinoside, quercetin 3-O-arabinoside and kaempferol.

3.1.2.5. Identification of flavonone flavonoids.

Peak **194** exhibited the precursor $[M-H]^-$ ion at m/z 255.0662 and yielded characteristic ions at m/z 135.007 $[C_7H_3O_3]^-$, 91.017 $[C_7H_3O_3-CO_2]^-$, and 119.048 $[C_8H_7O]^-$ obtained due to RDA cleavage, suggesting that it was characterized as liquiritigenin by comparison with OTCML database. Moreover, peaks **69**, **71**, **100**, **113**, **116**, **118**, **122**, **123**, **160**, **178**, **182** were considered as liquiritigenin-O-diglucuronide, glucoliquirtin asioside, liquiritigenin-O-diglucuronide, liquiritigenin-O-diglucuronide, liquiritin apioside, neoliquiritin, 1,1,3,4,5,6,8,8′-Octahydroxy-9H,9′H-2,2′-bixanthene-9,9′-dione, liquiritin, hydroxyliquiritin apioside, liquiritigenin-4′-O-(β-D-3-O-acetyl-apiofuranosyl-(1 → 2)-β-D-glucopyranoside, 6′-acetylliquiritin in accordance with the reference literatures (Wang et al., 2020; Xue et al., 2021). Peak **221** showed protonated molecular ion at m/z 271.0611, which produced characteristic fragment ions at m/z 151.002 $[C_7H_3O_4]^-$, 119.049 $[C_8H_7O]^-$ due to RDA cleavage. Therefore, peak **221** was identified as naringenin by comparison with reference standard along with the retention and the characteristic product ions. Meanwhile, based on similar fragmentation patterns, peaks **109**, **117**, **119**, **147**, **164**, **167**, **175**, **230** were identified as naringenin-4′-O-glucoside, eriocitrin, naringenin-5-O-glucoside, naringin, naringenin-7-O-glucoside, hesperidin, hesperetin-7-O-β-D-glucosidehesperetin.

3.1.2.6. Identification of isoflavone flavonoids.

Peak **213** generated the $[M + H]^+$ ion at m/z 301.0706, and the MS^2 spectrum showed fragment ions at m/z 286.046 $[M + H-CH_3]^+$, 258.054 $[M + H-CH_3-CO]^+$, 168.005 $[C_7H_4O_5]^+$, which allowed its identification as tectorigenin by comparison with the OTCML database. Based on similar fragmentation patterns, peaks **111**, **172**, **185**, **191**, **206**, **226**, **251**, **258**, **259** were respectively deduced as daidzin, tectoridin, ononin, glycitein, calycosin-7-O-β-D-glucoside, iristectorigenin B, Gancaonin N, biochanin A and glicoricone according to OTCML database.

3.1.3. Identification of triterpenoid saponins

In this study, a total of 28 saponins primarily derived from GU were characterized in ZKMG. Saponins are composed of a sapogenin of 3α-hydroxy oleanolic acid and sugar residues, such as glucose (Glc), glucuronic acid (GluA), rhamnose (Rha), and xylose (Xyl), which is mainly regarded as structure of 11-oxo-12-ene, 12-ene skeleton (Cheng et al., 2021). The proposed fragmentation pathway of glycyrrhizic acid (peaks **242**) was observed in Supplementary Figure S3.

Peak **242** showed precursor ion $[M-H]^-$ at m/z 821.3965, and its primary characteristic ions appeared at m/z 351.057 $[2GluA-H]^-$, 193.034 $[GluA-H]^-$ and 175.024 $[GluA-H_2O-H]^-$. Therefore, it was exactly identified as glycyrrhizic acid by comparing the retention time and fragmentation patterns with reference standard. Peaks **198**, **217**, **232**, **237**, **243**, **247**, which eluting at retention time of 13.35, 13.72, 14.11, 14.22, 14.38, 14.60 min respectively, exhibited the same molecular ion at m/z 837.39142 and the main fragment ions at m/z 351.057 $[2GluA-H]^-$, 193.034 $[GluA-H]^-$ and 175.024 $[GluA-H_2O-H]^-$. Thus, they were respectively deduced as yunganoside K2, licoricesaponin P2, licoricesaponin Q2, uralsaponin N, hydroxyglycyrrhizin, hydroxyglycyrrhizin based on their MS^2 fragmentation behavior, chromatographic retention time, and comparison with the similar known compounds and other reference evidence (Wang et al., 2020). Likewise, peaks **197**,

207, **209**, **211**, **215**, **216**, **218**, **222**, **227**, **231**, **233**, **238**, **242**, **248**, **249**, **260**, **265** were respectively as 24-hydroxy-licoricesaponin A3, licoricesaponin A3, 22-hydroxy-licoricesaponin G2 isomer 1, hydroxy acetoxyglycyrrhizin, 22-hydroxy-licoricesaponin G2 isomer 2, acetoxy-glycyrrhizic acid, methyllicorice-saponin Q2 isomer 1, yunganoside M, acetoxy-glycyrrhizic acid, licoricesaponin E2, methyllicorice-saponin Q2 isomer 2, acetoxyglycyrrhaldehyde, glycyrrhizic acid, licoricesaponin H2, licoricesaponin B2, 22-dehydro ural-saponin C, 18 β-glycyrrhetintic acid according to their similar fragmentation patterns, standard, OTCML database. Peak **255** gave a precursor ion $[M-H]^-$ at m/z 953.4751, which yielded characteristic fragment ions at m/z 497.115 $[2GluA + Rha-H]^-$, 435.114 $[2GluA + Rha-H_2O-CO_2-H]^-$, 339.093 $[GluA + Rha + H_2O-H]^-$, 321.082 $[GluA + Rha-H]^-$. Compared with the data in literatures, peak **255** was assigned as yunganoside D1 (Ji et al., 2014). Similarly, peak **234**, **246**, **250**, **252** were respectively characterized as haoglycyrrhizin isomer 1, haoglycyrrhizin isomer 2, yunganoside C1, yunganoside A1 based on their analogous fragmentation pathway and published data (Ji et al., 2014; Xue et al., 2021).

3.1.4. Identification of phenolic acids

In this research, a total of 27 phenolic acids were characterized. The proposed fragmentation pathway of ellagic acid (peaks **128**) was observed in Supplementary Figure S3. Peak **2**, **4**, **6**, **17**, **65**, **99**, **128**, **151** were exactly and respectively identified as quinic acid, malic acid, citric acid, gallic acid, caffeic acid, 4-coumaric acid, ellagic acid and salicylic acid with the reference standards. Peaks **3**, **5**, **6** indicated the same parent $[M-H]^-$ ion at m/z 191.0197, could give main product ions at m/z 173.008 $[M-H-H_2O]^-$, 129.018 $[M-H-H_2O-CO_2]^-$, 111.007 $[M-H-2H_2O-CO_2]^-$. Based on their chromatographic elution orders, further MS^2 fragmentation patterns and reported literature (Al Kadhi et al., 2017). Peaks **7**, **12**, **15** exhibited the same precursor ion $[M-H]^-$ at m/z 331.0670, which produced daughter ions at m/z 271.046 $[M-H-C_2H_4-O_2]^-$, 211.024 $[M-H-2C_2H_4O_2]^-$ and 169.013 $[M-H-C_6H_{10}-O_5]^-$ by loss of a glucose moiety. Based on similar fragmentation patterns and chromatographic elution orders, they were respectively identified as 1-O-galloylglucose, gallic acid-4-O-β-D-glucopyranoside, gallic acid-3-O-β-D-glucopyranoside (Jin et al., 2007). Peak **19** showed the similar protonated molecular ion at m/z 179.0349 with peak **65**, and yielded characteristic ion at m/z 135.044 $[M-H-CO_2]^-$, so it was presumed to be caffeic acid isomer. Peaks **20**, **22**, **35**, **41** were tentatively identified as danshensu, protocatechuic acid, coumaric acid, 4-hydroxybenzoic acid, respectively according to the OTCML database. Peaks **52**, **62**, **76** with the same protonated molecular ion $[M-H]^-$ at m/z 325.0928, were glucose moiety more than peak **35**, which produced characteristic ions at m/z 163.039 $[M-H-C_6H_{10}O_5]^-$, 145.028 $[M-H-C_6H_{10}O_5-H_2O]^-$ and 119.049 $[M-H-C_6H_{10}O_5-CO_2]^-$. Their fragment patterns were similar with peak **35**, so they were tentatively assigned as coumaric acid-O-glucose. Peak **126** exhibited $[M-H]^-$ ion at m/z 537.1038 and fragment behaviors are similar with lithospermic acid while retention time could not bring into correspondence with standard. Thus, it was tentatively assigned to lithospermic acid isomer. Peak **156** showed precursor ion $[M-H]^-$ at m/z 519.1871 and yielded characteristic ions at m/z 357.134 $[M-H-C_6H_{10}O_5]^-$, 151.039 $[C_8H_7O_3]^-$, indicat-

ing that peak **156** was inferred as pinoresinol 4-O-β-D-glucopyranoside. Peak **193** generated the quasi-molecular ion [M−H]⁻ at m/z 593.1875 and fragment ions at m/z 309.077 and 285.076. Thus, it was tentatively characterized as didymin. Peak **21** showed protonated molecular ion at m/z 329.0878, and produced fragment ions at m/z 167.034 [M−H−$C_6H_{10}O_5$]⁻, 152.010 [M−H−$C_6H_{10}O_5$−CH_3]⁻ and 123.044 [M−H−$C_6H_{10}O_5$−CO_2]⁻, suggesting that it was pseudolaroside B. Peaks **34** and **38** exhibited the same precursor ion [M−H]⁻ at m/z 285.0615, and it could form the fragment ions m/z 153.018 [M−H−$C_5H_8O_4$]⁻ by loss of an arabinose group and 109.028 [M−H−$C_5H_8O_4$−CO_2]⁻, suggesting that they were uralenneoside isomers.

3.1.5. Identification of phenylpropanoids

A total of 24 phenylpropanoids comprising of 4 coumaroylquinic acids, 3 feruloylquinic acids, 11 caffeylquinic acids and 6 other type acids were identified in ZKMG extract. The proposed fragmentation pathway of rosmarinic acid (peaks **170**) was observed in Supplementary Figure S3. Peaks **31**, **53**, **55**, **141**, **145**, **150**, **154**, **168**, **170** were exactly identified as neochlorogenic acid, chlorogenic acid, cryptochlorogenic acid,

acteoside, isochlorogenic acid B, 1,5-dicaffeoylquinic acid, isochlorogenic acid A, isochlorogenic acid C, rosmarinic acid, respectively. Likewise, peak **73** gave precursor ion [M−H]⁻ at m/z 515.1194, with the fragment ions at m/z 353.088 [M−H−caffeoyl]⁻, 191.055 [quinic acid-H]⁻, 179.034 [caffeic acid-H]⁻, 135.044 [caffeic acid-H-CO_2]⁻, which were consistent with the corresponding ions of dicaffeoylquinic acids. Therefore, peak **73** was inferred as dicaffeylquinic acid. Peaks **28**, **43**, **49** with the same parent ion [M−H]⁻ at m/z 515.1406 were a glucose group ($C_6H_{10}O_5$ 162.052 Da) more than peaks **31**, **53**, **55** and possessed similar characteristic fragment ions at m/z 173.044 [quinic acid-H-H_2O]⁻, 191.055 [quinic acid-H]⁻, 179.034 [caffeic acid-H]⁻ and 135.044 [caffeic acid-H-CO_2]⁻. Thus, they were tentatively identified as chlorogenic acid-hexosides. Peaks **47**, **75**, **82**, **97** were found to elute at 5.74, 7.17, 7.55, 8.60 min, with [M−H]⁻ ion at m/z 337.0928, and they could yield characteristic fragment ions at m/z 163.039 [coumaric acid-H]⁻, 119.048 [coumaric acid-H-CO_2]⁻, 191.055 [quinic acid-H]⁻, 173.044 [quinic acid-H-H_2O]⁻, suggesting that these compounds might be coumarylquinic acid. Therefore, Peaks **47**, **75**, **82**, **97** were respectively identified as 5-p-coumaroylquinic acid, 3-p-coumaroylquinic acid, 4-p-
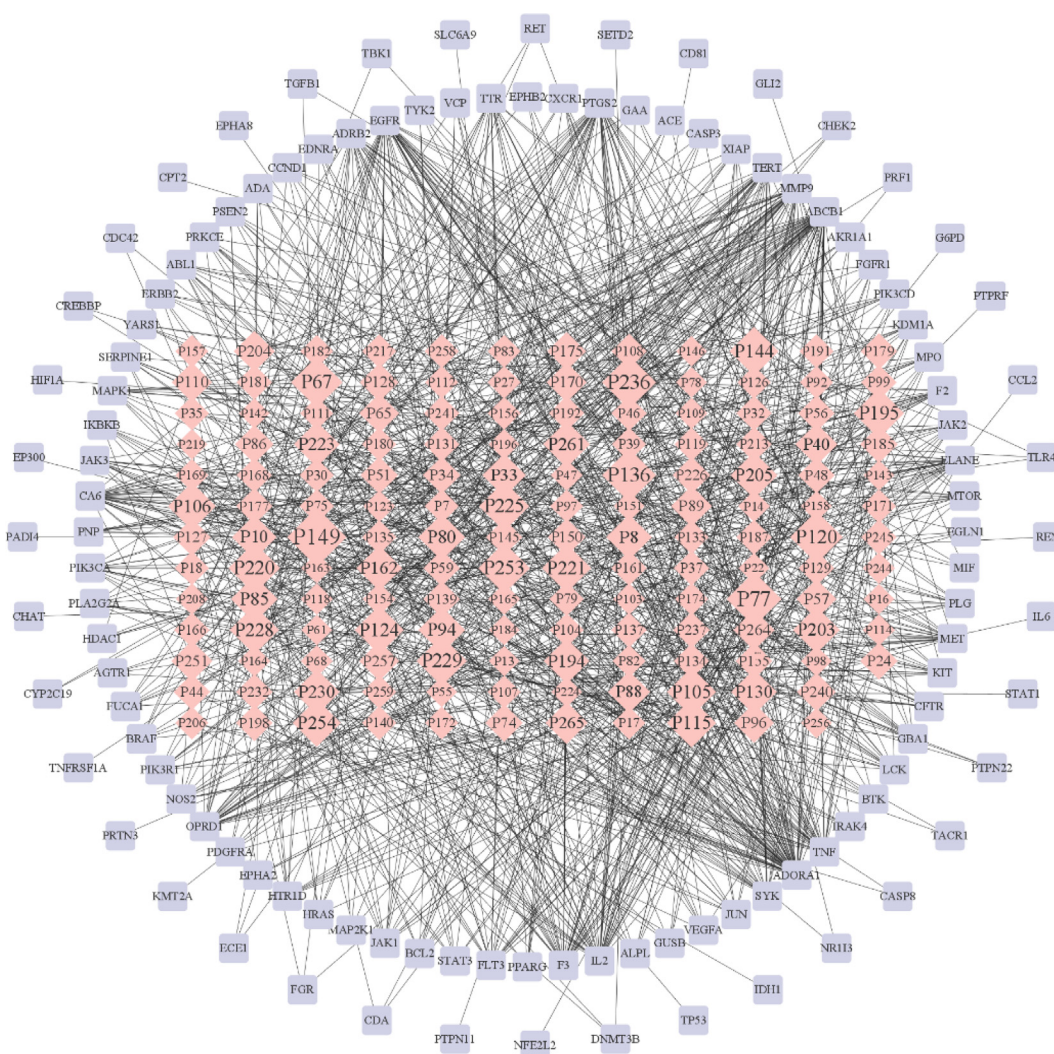
Fig. 3 Compound-target network. pink rhombus nodes represent compounds, and purple rectangular nodes represent targets.

coumaroylquinic acid, 1-p-coumaroylquinic acid according to their chromatographic elution behavior (Zhao et al., 2014). Peaks **59**, **92**, **107** were respectively eluted at 6.55, 8.39, 8.96 min with the parent ion $[M-H]^-$ at m/z 367.1034 and displayed characteristic secondary fragments at m/z 193.050 [ferulic acid-H]$^-$, 149.059 [ferulic acid-H-CO$_2$]$^-$, 134.036 [ferulic acid-H-CO$_2$-CH$_3$]$^-$, 173.044 [quinic acid-H-H$_2$O]$^-$, suggesting that these compounds might be feruloylquinic acid. Hence, they were tentatively identified as 4-feruloylquinic acid, 5-feruloylquinic acid, 3-feruloylquinic acid based on their chromatographic elution orders, further MS^2 fragmentation patterns and reported literature (Zheleva-Dimitrova et al., 2017). Peak **29** with the precursor ion $[M-H]^-$ at m/z 311.0408, gave characteristic product ions at m/z 149.008 [tartaric acid-H]$^-$, 179.034 [caffeic acid-H]$^-$, 135.044 [caffeic acid-H-CO$_2$]$^-$, suggesting that it was tentatively assigned to caftaric acid according to the OTCML database. Peak **40** was tentatively identified as esculin based on the OTCML database. Peak **195** with the parent ion $[M-H]^-$ at m/z 373.0928, was methyl (CH$_2$ 14.015 Da) more than peak **170**, and produced characteristic ions at m/z 197.045 [M-H-C$_9$H$_7$O$_3$]$^-$, 179.034 [M-H-C$_9$H$_9$O$_4$]$^-$, 161.023 [M-H-C$_9$H$_9$O$_4$-H$_2$O]$^-$, 135.044 [M-H-C$_9$H$_9$O$_4$-CO$_2$]$^-$, which were the same fragment patterns as peak **170**. Therefore, it was identified as methyl ros-

marinate based on the OTCML database. Peaks **141**, **152** both gave precursor ion $[M-H]^-$ at m/z 623.1981, and yielded fragment ions at m/z 461.166 [M-H-C$_9$H$_6$O$_3$]$^-$, 179.034 [C$_9$H$_7$O$_4$]$^-$, 161.023 [C$_9$H$_7$O$_4$-H$_2$O]$^-$, 135.043 [C$_9$H$_7$O$_4$-CO$_2$]$^-$, suggesting that they were a group of isomers. Peak **141** was confirmed as acteoside by standard, so peak **152** was identified as isoacteoside based on their chromatographic retention behavior.

3.1.6. Identification of anthraquinones

A total of 21 quinones were identified in ZKMG, including 3 rheic acid-types, 3 physcion-types, 3 emodin-types, 6 chrysophanol-types, 3 aurantio-obtusin-types, 2 aloe-emodin-types and 1other compound, which are all derived from RP. The proposed fragmentation pathway of rhein (peak **256**) was observed in **Supplementary Figure S3**.

Peaks **208**, **256**, **264** were unambiguously attributed to physcion, rheic acid, emodin by comparison with the authentic standards. Rhein as the main anthraquinone in ZKMG, was used to characterize the fragmentation pathways. It exhibited a parent ion $[M-H]^-$ at m/z 283.0248, and yielded characteristic product ions at m/z 255.030 [M-H-CO]$^-$, 239.034 [M-H-CO$_2$]$^-$, 211.039 [M-H-CO$_2$-CO]$^-$, 183.044 [M-H-CO$_2$-2CO]$^-$. Based on these fragmentation patterns,
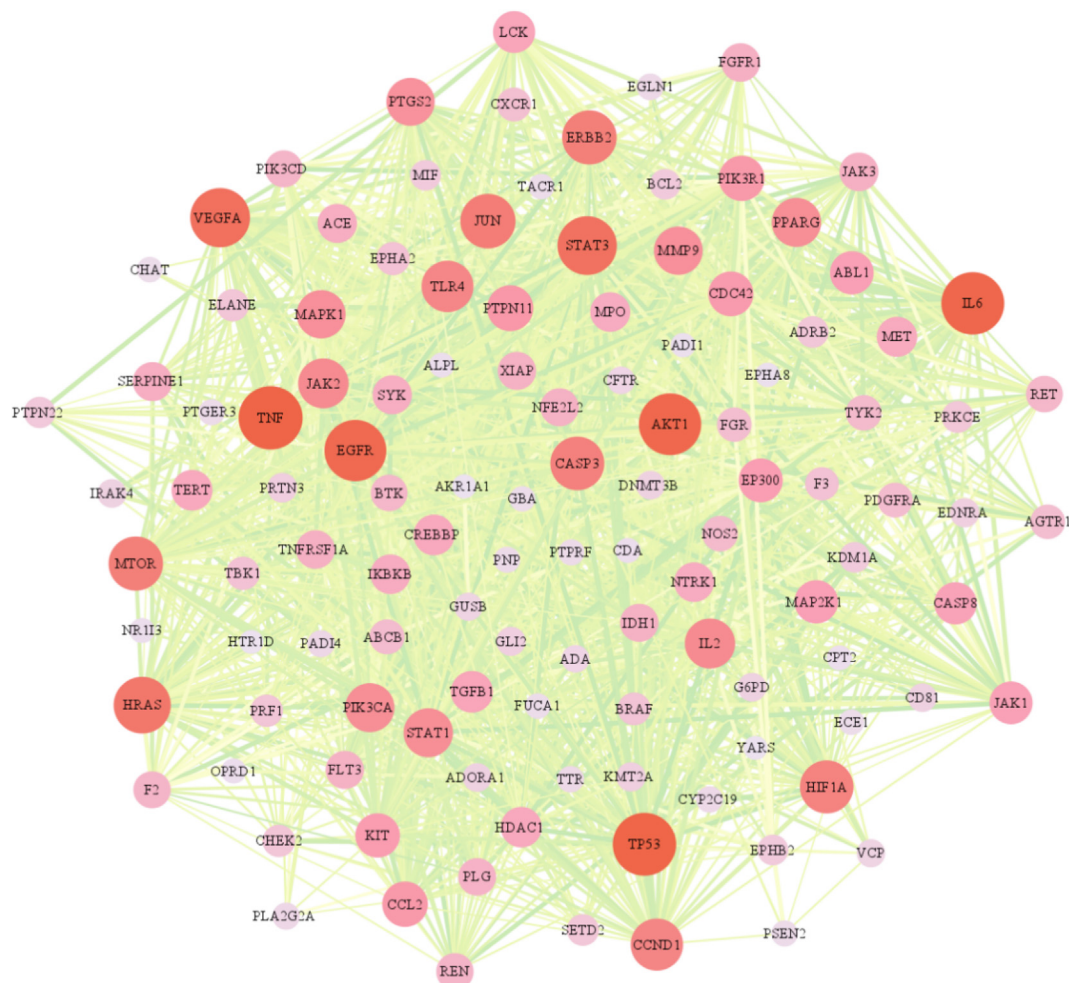
Fig. 4 Protein-protein interaction (PPI) network.

peaks **138**, **254** were identified as rhein-8-O-β-D-glucoside and 6-methyl-rhein. Physcion showed a precursor ion [M−H]⁻ at m/z 283.0611, which produced characteristic ions at m/z 268.037 [M−H−CH$_3$]⁻, 240.042 [M−H−CH$_3$−CO]⁻. Therefore, peaks **219**, **224** were respectively identified as physcion-8-O-β-D-glucoside and physcion-1-O-β-D-glucoside according to the chromatographic elution orders, similar fragment patterns. Emodin indicated the parent ion [M−H]⁻ at m/z 269.0455, and produced product ions at m/z 241.050 [M−H−CO]⁻, 225.054 [M−H−CO$_2$]⁻. Based on these fragmentation patterns, peaks **165**, **202** were identified as emodin-1-O-D-glucoside and emodin-8-O-D-glucoside. Likewise, peaks **102**, **173**, **177**, **184**, **190**, **196**, **204**, **205**, **212**, **241**, **244**, **262** were assigned to carboxyl-chrysophanol-O-glucose, aurantio-obtusin-6-O-rutinoside, aloe-emodin-3-(hydroxymethyl)-O-β-D-glucopyranoside, aurantio-obtusin-6-O-glucoside, carboxyl-chrysophanol-O-glucose, aloe-emodin-8-O-(6-O-acetyl)-glucoside, chrysophanol-1-O-β-D-glucoside, chrysophanol, chrysophanol-8-O-glucoside, aurantio-obtusin, chrysophanol-O-acetylglucoside, 1-Methyl-8-hydroxy-9,10-anthraquinone-3-O-(6'-O-cinnamoyl)-glucoside, respectively, according to the similar fragment patterns.

3.1.7. Identification of tannins

Tannins might exist in ZKMG as they are important compounds found in the crude drug RP. Totally, 13 tannins were identified in ZKMG extract. The proposed fragmentation pathway of tri-O-galloyl-glucoside (peaks **54**) was observed in **Supplementary Figure S3**. Peaks **54**, **63**, **66**, **81**, **84**, **90**, **93** gave the precursor [M−H]- ion at m/z 635.0889, and produced characteristic ions at m/z 483.077 [M−H−C$_7$H$_4$O$_4$]⁻, 465.067 [M−H−C$_7$H$_4$O$_4$−H$_2$O]⁻, 313.057 [M−H−2C$_7$H$_4$O$_4$−H$_2$O]⁻, 169.013 [C$_7$H$_5$O$_5$]⁻, and 125.023 [C$_7$H$_5$O$_5$-CO$_2$]⁻, thus they were assigned as tri-O-galloyl-glucoside isomers. According to this method, peaks **26**, **36**, **42**, **45**, **50**, **60** were identified as gallic acid-O-galloyl-glucoside isomers.

3.1.8. Identification of other compounds

The other compounds including 4 amino acids, 2 naphthols, 2 phenols, 2 terpenoids were detected in ZKMG. The proposed fragmentation pathway of brervifolincaboxylic acid (peak **58**) was observed in **Supplementary Figure S3**. Peaks **1** and **13** were confirmed as adenine and adenosine cyclophosphate, respectively, compared with known reference compounds. Peaks **9** and **11** both showed [M + H]⁺ at m/z 132.1019, and gave
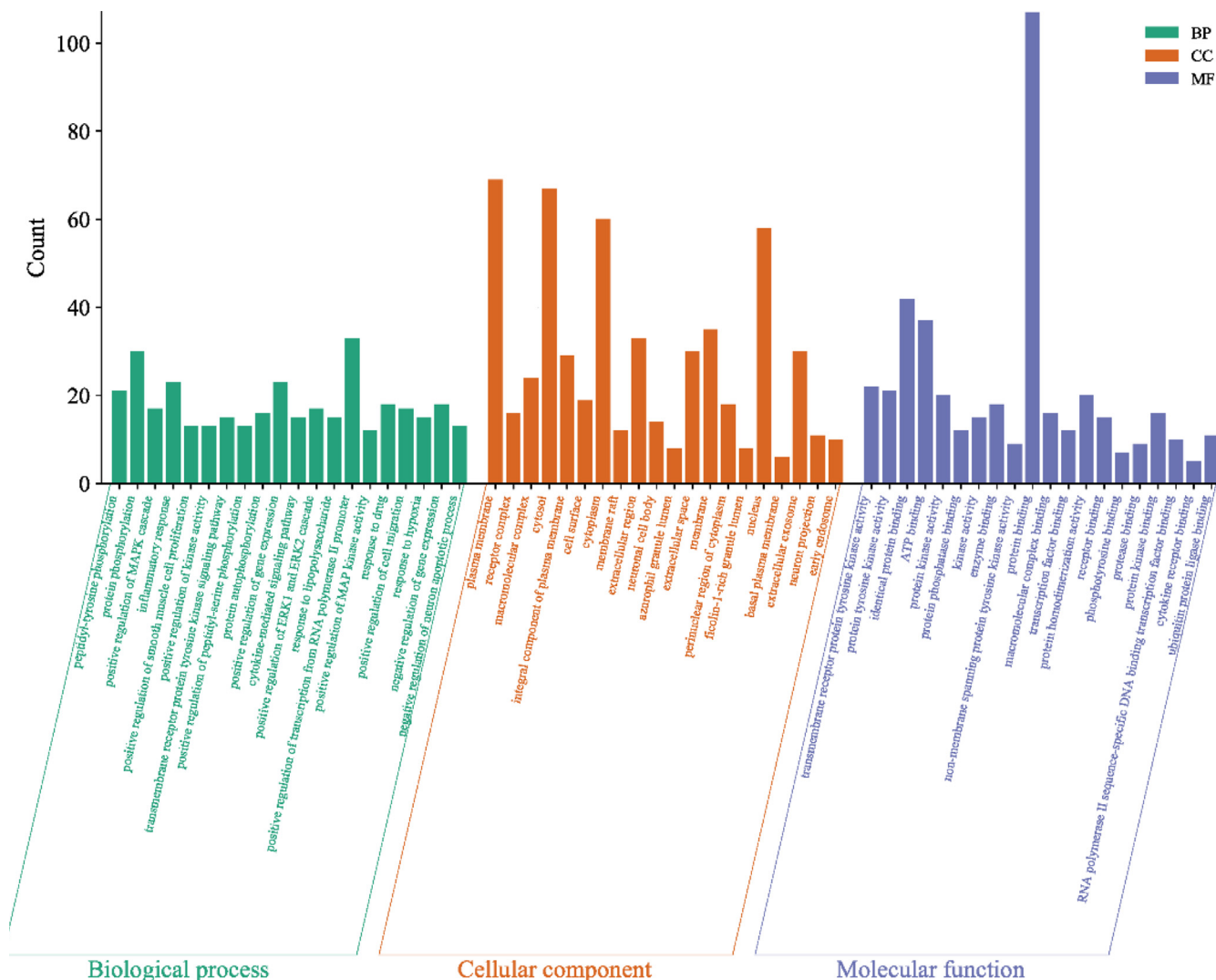
Fig. 5   GO term histograms.

the same MS^2 fragmentation ion at m/z 86.096 [M + H-CO-H$_2$O]$^+$, indicating that they were isomers. Consequently, peaks **9** and **11** were respectively characterized as isoleucine, leucine based on chromatographic elution orders. Peak **200** exhibited a precursor ion [M−H]$^-$ at m/z 407.1347, and showed the product ions at m/z 245.081[M-H-C$_6$H$_{10}$O$_5$]$^-$ by loss of a glucosyl group, 230.058 [M−H−C$_6$H$_{10}$O$_5$−CH$_3$]$^-$ by elimination of a CH$_3$ radical. Hence, it was identified as torachrysone-8-O-glucoside. Peak **239** with the parent ion [M−H]$^-$ at m/z 449.1453, was acetyl (C$_2$H$_2$O 42.010 Da) more than peak **200**, and yielded the same fragment ions. Thus, it was tentatively characterized as torachrysone-O-acetylglucoside. Peak **58** showed [M−H]$^-$ ion at m/z 291.0146, and gave MS^2 fragmentation ions at m/z 247.024 [M−H−CO$_2$]$^-$, 219.029 [M−H−CO$_2$−CO]$^-$, 191.034 [M−H−CO$_2$−2CO]$^-$, 173.023 [M−H−CO$_2$−2CO−H$_2$O]$^-$, suggesting that it was identified as brevifolincaboxylic acid (Chen et al., 2022). Besides, peaks **8**, **10**, **18**, **23**, **25**, **78**, **253** were respectively characterized as adenosine, guanosine, phenylalanine, 3,4-dihydroxyphenylethanol, tryptophan, camphor, steviol-19-O-glucoside based on the OTCML database.

3.2. Network pharmacology analysis

3.2.1. Potential bioactive compounds and targets of ZKMG in the treatment of AURTIs

In this study, UHPLC-MS was used to detect a total of 265 chemical components of ZKMG. By searching the Swiss Target Prediction, 836 targets were obtained from identified compounds, and 1317 AURTIs related targets based on OMIM and GeneCards database (**Supplementary Table S3**). Finally, 120 overlapping targets were obtained by precisely matching

the potential targets of the above two steps through the online tool Venny 2.1, suggested that ZKMG would play a role in treating AURTIs associated with these 120 common targets (**Supplementary Figure S4**).

3.2.2. Compound target network analysis

The active ingredient potential target network of ZKMG in (Fig. 3). There are 271 nodes and 1117 edges in the network, among which the 155 pink nodes represent the main components of ZKMG, the 116 purple nodes represent the targets of AURTIs, and 1117 edges represent the interactions between the components and the targets of AURTIs. The size of the compounds in the network increases with the number of edges (degree of targets). The fact that the same active ingredient can act on multiple targets and the same target also corresponds to different chemical components were observed from the network, which fully reflect the multicomponent and multitarget characteristics of ZKMG in the treatment of AURTIs. The compounds were screened with a degree and betweenness centrality greater than the mean, such as 18 β-Glycyrrhetintic acid, noscapine, n-methylnarcotine, adenosine, methyl rosmarinate, thebaine, 6-methyl-rhein, which were possibly potential active ingredients of ZKMG in the treatment of AURTIs.

3.2.3. PPI network analysis

STRING analysis was used to compare 120 overlapping targets and produce a PPI network, as well as the visualization was realized by Cytoscape software (Fig. 4). There were 117 nodes and 1562 edges were observed with a combined score of greater than 0.4 (**Supplementary Table S4**). The size and color of the node reflected the importance of the degree. The larger the degree, the more important the node is in the net-
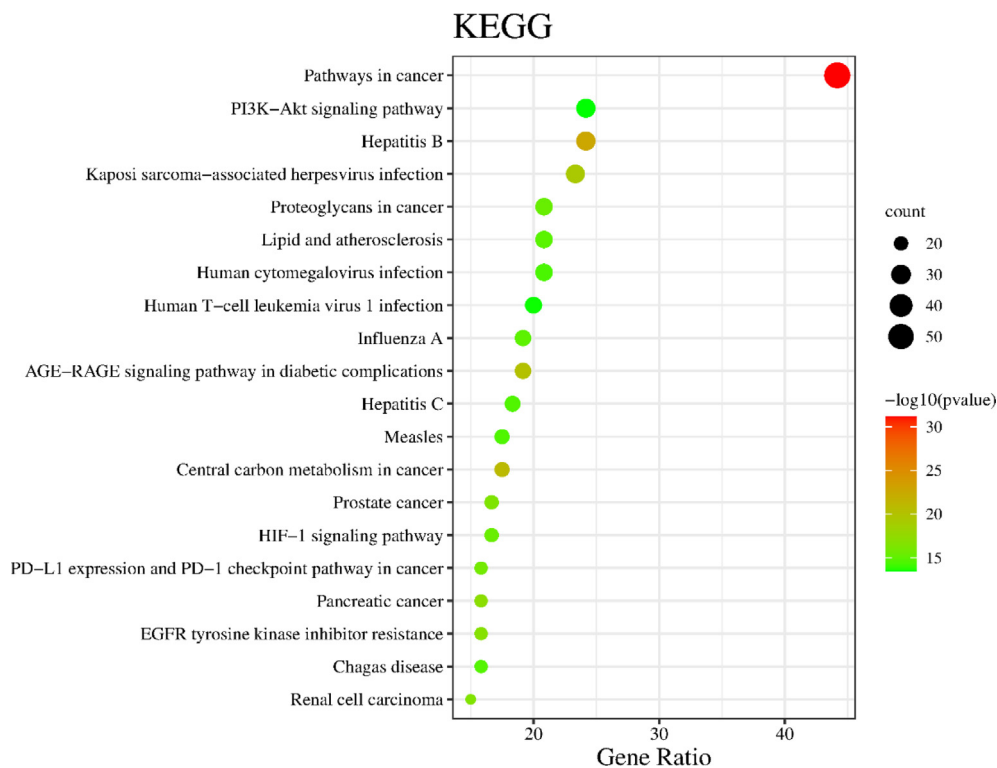
Fig. 6 Bubble map of KEGG pathway analysis.
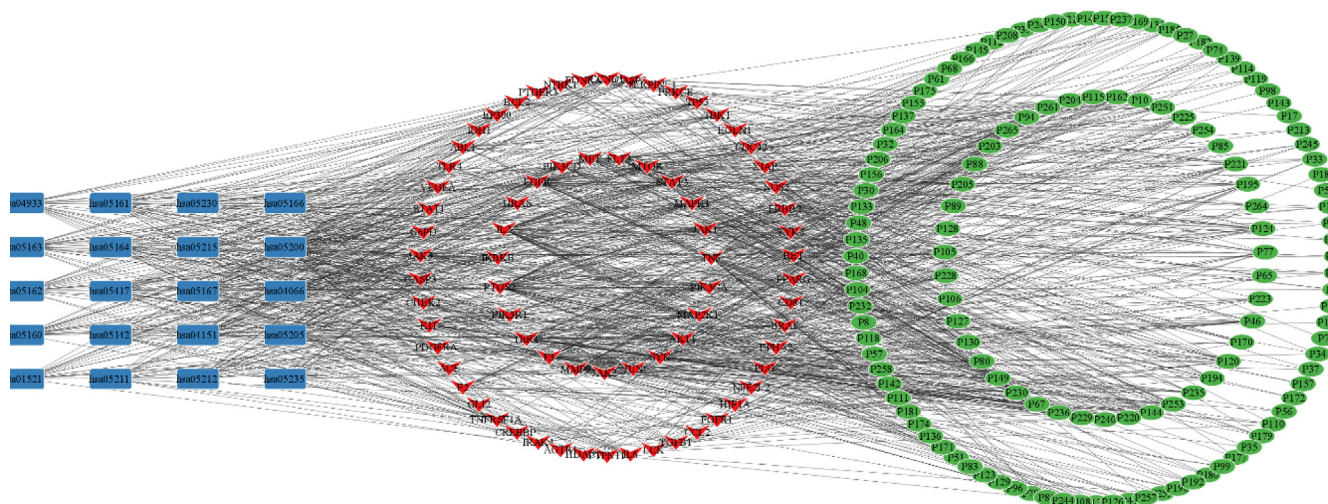
Fig. 7 Compound-target-pathway network. green circular nodes represent chemical compounds, red V-shaped nodes represent targets, and blue rectangular nodes represent pathways.

work, suggesting that it may be a key target of ZKMG in the treatment of AURTIs. The top 10 nodes were selected as the major genes, including TNF, TP53, IL6, AKT1, EGFR, VEGFA, STAT3, HRAS, JUN, ERBB2, which were likely to be the critical genes in the development of AURTIs.

3.2.4. GO analysis and KEGG pathway analysis

GO function and KEGG pathway analysis of the 120 candidate target genes were posted on the DAVID database to explore the molecular mechanism of ZKMG in treating AUR-TIs. GO evaluations were illustrated by using biological process (BP), cell component (CC), and molecular function (MF) terms. The results of GO analysis showed that potential target genes were enriched, which involved with 638 pathways, including 505 BPs, 52 CCs and 81 MFs (P ≤ 0.05). The top 20 pathways of BP, CC, MF with the highest number of genes involved were shown in the Fig. 5. In BP, the targets mainly involved peptidyl-tyrosine phosphorylation, protein phosphorylation, inflammatory response. In CC, the targets mainly involved plasma membrane, receptor complex, macromolecular complex. In MF, the targets mainly involved transmembrane receptor protein tyrosine kinase activity, protein tyrosine kinase activity, identical protein binding, protein kinase activity (Supplementary Table S5). KEGG pathway annotation indicated that potential target genes were involved in 148 pathways (P ≤ 0.05). The top 20 KEGG pathways with the highest number of genes were shown in the Fig. 6, including PI3K-Akt signaling pathway, AGE-RAGE signaling pathway in diabetic complications, PD-L1 expression and PD-1 checkpoint pathway in cancer, HIF-1 signaling pathway (Supplementary Table S6).

3.2.5. Compound target pathway network analysis

In order to explore the key compounds of ZKMG in treating AURTIs, the top 20 KEGG pathways, corresponding targets and compounds were constructed to the component-target-pathways network as shown in Fig. 7. The network contained 227 nodes with 134 representative components, 73 representative targets, 20 representative pathways, and 1193 edges. The results indicated that alkaloids mainly derived from PP played

an important role in the treatment of ZKMG in treating AUR-TIs due to their higher degrees, such as noscapine (degree = 24), cryptopine (degree = 17), N-methylnarcotine (degree = 16), allocryptopine (degree = 15). In addition, the targets and active components were distributed in different pathways and played a key role in the treatment of AURTIs, which profoundly reflected the multicomponent, multitarget, and multipathway features of TCM.

4. Conclusion

In this study, a rapid and sensitive UHPLC-Q-Exactive Orbitrap-MS method combined with network pharmacology was established to characterize pharmacodynamic Substance and predict potential molecular mechanisms of ZKMG in treating AURTIs. Finally, a total of 265 were identified or tentatively characterized including 46 alkaloids, 92 flavonoids, 28 triterpenoid saponins, 27 phenolic acids, 24 phenylpropanoids, 21 quinones, 13 tannins, 4 amino acids, 4 nucleosides, 2 naphthols, 2 phenols and 2 terpenoids. Based on the pharmacological network analysis of compound target pathway, EGFR, PTGS2, IL2, MMP9, TNF, AKT1, PIK3CA and F3 were regarded as key targets for ZKMG to exhibit its effects against AURTIs. Alkaloids, flavonoids, phenylpropanoids and terpenoids such as noscapine, cryptopine, steviol-19-O-glucoside, N-methylnarcotine, methyl rosmarinate, allocryptopine, naringenin and boldine indicated that multiple compounds possessed comprehensive activities by interacting with the above targets against AURTIs. In conclusion, the result revealed that the relationship between compounds and effects of ZKMG treated the AURTIs as well as could lay the foundation of quality control research and clinical application of ZKMG in the future. However, the effective constituents, active targets, and signaling pathways obtained based on UHPLC-MS and network pharmacology need to be confirmed and validated by animal experiment in further studies.

Declaration of Competing Interest

The authors declare that they have no known competing financial interests or personal relationships that could have appeared to influence the work reported in this paper.

Appendix A. Supplementary material

Supplementary data to this article can be found online at https://doi.org/10.1016/j.arabjc.2023.104875.

References

Al Kadhi, O., Melchini, A., Mithen, R., Saha, S., 2017. Development of a LC-MS/MS method for the simultaneous detection of tricarboxylic acid cycle intermediates in a range of biological matrices. J. Anal. Methods Chem., 5391832

Alrafiaah, A.S., Alqarny, M.H., Alkubedan, H.Y., AlQueflie, S., Omair, A., 2017. Are the Saudi parents aware of antibiotic role in upper respiratory tract infections in children? J. Infect. Public Heal. 10 (5), 579–585.

Amberger, J.S., Bocchini, C.A., Schiettecatte, F., Scott, A.F., and Hamosh, A., 2015. OMIM.org: Online Mendelian Inheritance in Man (OMIM®), an online catalog of human genes and genetic disorders. Nucleic Acids Res. 43 (Database issue), D789-798

Chen, W., He, L., Zhong, L., Sun, J., Zhang, L., Wei, D., 2021. Identification of active compounds and mechanism of Huangtu Decoction for the treatment of ulcerative colitis by network pharmacology combined with experimental verification. Drug Des. Devel. Ther. 15, 4125–4140.

Chen, L.M., Talaiti, Zulipiya., Aili, Yusufujiang., Li, J.M., Huo, S.X., Gao, H.M. Establishment of a quality control method for simultaneous determination of multiple active components in Uygur medicine of nymphaeae flos. Chin J Exp Tradit Med Formulae. 1-10.

Cheng, M., Yao, C., Li, Y., Li, Z., Li, H., Yao, S., 2021. A strategy for practical authentication of medicinal plants in traditional Chinese medicine prescription, paeony root in ShaoYao-GanCao decoction as a case study. J. Sep. Sci. 44 (12), 2427–2437.

Conceição, R.S., Reis, I.M.A., Cerqueira, A.P.M., Perez, C.J., Junior, M., Branco, A., 2020. Rapid structural characterisation of benzylisoquinoline and aporphine alkaloids from Ocotea spixiana acaricide extract by HPTLC-DESI-MS(n). Phytochem. Anal. 31 (6), 711–721.

Daina, A., Michielin, O., Zoete, V., 2019. SwissTargetPrediction: updated data and new features for efficient prediction of protein targets of small molecules. Nucleic Acids Res. 47 (W1), W357–W364.

Fiore, C., Eisenhut, M., Krausse, R., Ragazzi, E., Pellati, D., Armanini, D., 2008. Antiviral effects of Glycyrrhiza species. Phytother. Res. 22 (2), 141–148.

Harris, A.M., Hicks, L.A., Qaseem, A., 2016. Appropriate antibiotic use for acute respiratory tract infection in adults: advice for High-Value care from the American college of physicians and the centers for disease control and prevention. Ann. Intern. Med. 164 (6), 425–434.

Hou, S.H., Huang, F., Li, J.J., Yin, Q., Zhang, D.N., Wang, Q., 2019. Analysis of anti-inflammation mechanism of Zukamu granules based on network pharmacology and HS-SPME-GC-MS. J. Int. Pharm. Res. 46 (06), 441–455.

Huang da, W., Sherman, B.T., Lempicki, R.A., 2009. Systematic and integrative analysis of large gene lists using DAVID bioinformatics resources. Nat. Protoc. 4 (1), 44–57.

Huang, Z., Pan, X., Zhou, J., Leung, W.T., Li, C., and Wang, L., 2019. Chinese herbal medicine for acute upper respiratory tract infections and reproductive safety: A systematic review. BioScience Trends. advpub

Huang, Q., Zhang, F., Liu, S., Jiang, Y., Ouyang, D., 2021. Systematic investigation of the pharmacological mechanism for renal protection by the leaves of Eucommia ulmoides Oliver using UPLC-Q-TOF/MS combined with network pharmacology analysis. Biomed. Pharmacother. 140, 111735.

James, S.L., Abate, D., Abate, K.H., Abay, S.M., Abbafati, C., Abbasi, N., 2018. Global, regional, and national incidence, prevalence, and years lived with disability for 354 diseases and injuries for 195 countries and territories, 1990–2017: a systematic analysis for the Global Burden of Disease Study 2017. The Lancet 392 (10159), 1789–1858.

Jeong, E.K., Lee, S.Y., Yu, S.M., Park, N.H., Lee, H.S., Yim, Y.H., 2012. Identification of structurally diverse alkaloids in Corydalis species by liquid chromatography/electrospray ionization tandem mass spectrometry. Rapid Commun. Mass Spectrom. 26 (15), 1661–1674.

Ji, S., Wang, Q., Qiao, X., Guo, H.C., Yang, Y.F., Bo, T., 2014. New triterpene saponins from the roots of Glycyrrhiza yunnanensis and their rapid screening by LC/MS/MS. J. Pharm. Biomed. Anal. 90, 15–26.

Jin, W., Wang, Y.F., Ge, R.L., Shi, H.M., Jia, C.Q., Tu, P.F., 2007. Simultaneous analysis of multiple bioactive constituents in Rheum tanguticum Maxim. ex Balf. by high-performance liquid chromatography coupled to tandem mass spectrometry. Rapid Commun. Mass Spectrom. 21 (14), 2351–2360.

Kong, X., Liu, C., Lu, P., Guo, Y., Zhao, C., Yang, Y., 2021. Combination of UPLC-Q-TOF/MS and network pharmacology to reveal the mechanism of Qizhen Decoction in the treatment of colon cancer. ACS Omega 6 (22), 14341–14360.

Li, S., Liu, G., Gu, M., Li, Y., Li, Y., Ji, Z., 2022. A novel therapeutic approach for IPF: based on the "Autophagy-Apoptosis" balance regulation of Zukamu Granules in alveolar macrophages. J. Ethnopharmacol. 297, 115568.

Liu, Z., Ma, N., Zhong, Y., Yang, Z.Q., 2015. Antiviral effect of emodin from Rheum palmatum against coxsakievirus B5 and human respiratory syncytial virus in vitro. J. Huazhong Univ. Sci. Technol. Med. Sci. 35 (6), 916–922.

Lu, X., Zheng, Y., Wen, F., Huang, W., Chen, X., Ruan, S., 2021. Study of the active ingredients and mechanism of Sparganii rhizoma in gastric cancer based on HPLC-Q-TOF-MS/MS and network pharmacology. Sci. Rep. 11 (1), 1905.

Luo, J., Chen, G., Liu, D., Wang, Y., Qi, Q., Hu, H., 2019. Study on the material basis of Houpo Wenzhong decoction by HPLC fingerprint, UHPLC-ESI-LTQ-Orbitrap-MS, and network pharmacology. Molecules 24 (14).

Menéndez-Perdomo, I.M., Hagel, J.M., Facchini, P.J., 2021. Benzylisoquinoline alkaloid analysis using high-resolution Orbitrap LC-MS(n). J. Mass Spectrom. 56 (2), e4683.

Nakamura, T., Kinjo, C., Nakamura, Y., Kato, Y., Nishikawa, M., Hamada, M., 2018. Lymphatic metabolites of quercetin after intestinal administration of quercetin-3-glucoside and its aglycone in rats. Arch. Biochem. Biophys. 645, 126–136.

Oh, J.H., Ha, I.J., Lee, M.Y., Kim, E.O., Park, D., Lee, J.H., 2018. Identification and metabolite profiling of alkaloids in aerial parts of Papaver rhoeas by liquid chromatography coupled with quadrupole time-of-flight tandem mass spectrometry. J. Sep. Sci. 41 (12), 2517–2527.

Parsaei, D.P., Bahmani, M., Naghdi, N., Asadi-Samani, M., Rafieian-kopaei, M., Tajeddini, P., 2016. Identification of medicinal plants effective on common cold: an ethnobotanical study of Shiraz. South Iran. 8, 90–97.

Pelzman, F.N., Tung, J., 2021. A symptom-directed paradigm for the evaluation and management of upper respiratory tract infections. Med. Clin. North Am. 105 (1), 199–212.

Shannon, P., Markiel, A., Ozier, O., Baliga, N.S., Wang, J.T., Ramage, D., 2003. Cytoscape: a software environment for integrated models of biomolecular interaction networks. Genome Res. 13 (11), 2498–2504.

Song, Y., Su, D., Lu, T., Mao, C., Ji, D., Liu, Y., 2014. Differential pharmacokinetics and the brain distribution of morphine and ephedrine constitutional isomers in rats after oral administration with Keke capsule using rapid-resolution LC-MS/MS. J. Sep. Sci. 37 (4), 352–359.

Stelzer, G., Rosen, N., Plaschkes, I., Zimmerman, S., Twik, M., Fishilevich, S., 2016. The GeneCards Suite: From Gene Data Mining to Disease Genome Sequence Analyses. Curr Protoc Bioinformatics. 54, 1.30.31-31.30.33.

Szklarczyk, D., Gable, A.L., Lyon, D., Junge, A., Wyder, S., Huerta-Cepas, J., 2018. STRING v11: protein–protein association networks with increased coverage, supporting functional discovery in genome-wide experimental datasets. Nucleic Acids Res. 47 (D1), D607–D613.

UniProt Consortium, T., 2018. UniProt: the universal protein knowledgebase. Nucleic Acids Res. 46 (5), 2699

Wang, J., Wang, P., Wang, X., Zheng, Y., Xiao, Y., 2014. Use and prescription of antibiotics in primary health care settings in China. JAMA Intern. Med. 174 (12), 1914–1920.

Wang, Y.L., Zhang, C.C., Zhang, F., Huang, J., Wang, D.D., Zhao, Y.F., 2020. Chemical profiling and tissue distribution study of Jingyin Granules in rats using UHPLC-Q-Exactive Orbitrap HR-MS. China J. Chin. Mater. Med. 45 (22), 5537–5554.

Wang, X., Zhou, W., Wang, Q., Zhang, Y., Ling, Y., Zhao, T., 2021. A novel and comprehensive strategy for quality control in complex Chinese medicine formula using UHPLC-Q-Orbitrap HRMS and UHPLC-MS/MS combined with network pharmacology analysis: take Tangshen formula as an example. J. Chromatogr. B Analyt. Technol. Biomed. Life Sci. 1183, 122889.

Xu, X., Zhang, W., Wu, X., Sun, Y., Yang, H., Pu, Y., 2022. The effectiveness and safety of Chaiqin Qingning Capsule in upper respiratory tract infections with fever: a prospective, double-blinded, randomized, multicenter controlled trial. Complement. Ther. Med. 68, 102840.

Xue, X., Jiao, Q., Jin, R., Wang, X., Li, P., Shi, S., 2021. The combination of UHPLC-HRMS and molecular networking improving discovery efficiency of chemical components in Chinese Classical Formula. Chin. Med. 16 (1), 50.

Yang, R., Yu, B.Y., Liu, J.H., 2016. Recent research progress in the pharmacological effects of tetrahydroprotoberberines. Prog. Pharm. Sci. 40 (10), 739–744.

Zeng, L., Li, H., Zhang, C., Kang, D., Liu, G., Li, X., 2022. Effectiveness and safety of Danmu extract syrup for acute upper respiratory tract infection in children: a real-world, prospective cohort study. J. Evid. Based Med. 15 (1), 19–29.

Zeng, Y., Lou, G., Ren, Y., Li, T., Zhang, X., Wang, J., 2021. Network pharmacology-based analysis of Zukamu granules for the treatment of COVID-19. Eur. J. Integr. Med. 42, 101282.

Zhang, Y.Y., Xia, R.Y., Liang, S.B., Hu, X.Y., Dai, M.Y., Li, Y.L., 2021. Chinese patent herbal medicine (Shufeng Jiedu capsule) for acute upper respiratory tract infections: a systematic review and meta-analysis. Integr. Med. Res. 10, (3) 100726.

Zhao, T., He, J., Wang, X., Ma, B., Wang, X., Zhang, L., 2014. Rapid detection and characterization of major phenolic compounds in *Radix Actinidia* chinensis Planch by ultra-performance liquid chromatography tandem mass spectrometry. J. Pharm. Biomed. Anal. 98, 311–320.

Zhao, L., Ouyang, H., Wang, Q., Fan, D., Wang, Y., Yang, S., 2019. Chemical fingerprint analysis and metabolic profiling of 50% ethanol fraction of *Lomatogonium rotatum* by ultra-performance liquid chromatography/quadrupole-time of flight mass spectrometry. Biomed. Chromatogr. 33 (11), e4651.

Zheleva-Dimitrova, D., Gevrenova, R., Zaharieva, M.M., Najdenski, H., Ruseva, S., Lozanov, V., 2017. HPLC-UV and LC-MS Analyses of acylquinic acids in *Geigeria alata* (DC) Oliv. & Hiern. and their contribution to antioxidant and antimicrobial capacity. Phytochem. Anal. 28 (3), 176–184.

Zhuang, Z., Wen, J., Zhang, L., Zhang, M., Zhong, X., Chen, H., 2020. Can network pharmacology identify the anti-virus and anti-inflammatory activities of Shuanghuanglian oral liquid used in Chinese medicine for respiratory tract infection? Eur. J. Integr. Med. 37, 101139.